

Centralized Vs. Distributed Computer Systems for a Multi-Instrument Sounding Rocket
Payload

by

Patrick Bucknam Lokken

A thesis submitted in partial fulfillment
of the requirements for the degree

of

Master of Science

in

Electrical Engineering

MONTANA STATE UNIVERSITY
Bozeman, Montana

May 2011

©COPYRIGHT

by

Patrick Bucknam Lokken

2011

All Rights Reserved

APPROVAL

of a thesis submitted by

Patrick Bucknam Lokken

This thesis has been read by each member of the thesis committee and has been found to be satisfactory regarding content, English usage, format, citation, bibliographic style, and consistency and is ready for submission to The Graduate School.

Dr. Joseph A. Shaw

Approved for the Department of Electrical and Computer Engineering

Dr. Robert C. Maher

Approved for The Graduate School

Dr. Carl A. Fox

STATEMENT OF PERMISSION TO USE

In presenting this thesis in partial fulfillment of the requirements for a master's degree at Montana State University, I agree that the Library shall make it available to borrowers under rules of the Library.

If I have indicated my intention to copyright this thesis by including a copyright notice page, copying is allowable only for scholarly purposes, consistent with "fair use" as prescribed in the U.S. Copyright Law. Requests for permission for extended quotation from or reproduction of this thesis in whole or in parts may be granted only by the copyright holder.

Patrick Bucknam Lokken

May 2011

[DEDICATION, ACKNOWLEDGEMENTS, VITA - optional]

[Paragraphs are left block, indent first line. Dedication may be no longer than one page, single spaced. Acknowledgments must be double spaced.

If you include a vita, it should contain the full name of the author, date and place of birth, parentage, secondary education, and collegiate degrees. The vita should be written in essay form in the third person and may not exceed one single-spaced page.

Title of these pages should be in all caps.]

TABLE OF CONTENTS

1. CHAPTER ONE TITLE IN CAPS	1
First Level Heading.....	2
Another First Level Heading	3
Second Level Heading	4
Another Second Level Heading	5
Third Level Heading	6
2. CHAPTER TWO TITLE IN CAPS	7
First Level Heading.....	8
Second Level Heading	9
REFERENCES CITED	10
APPENDICES	11
APPENDIX A: Title of Appendix A in upper/lowercase	12
APPENDIX B: Title of Appendix B in upper/lowercase	13

TABLE OF CONTENTS - CONTINUED

LIST OF TABLES

[If list of tables continues to more than one page, the following pages must have a header: LIST OF TABLES – CONTINUED and include Table and Page titles.]

Table	Page
1. Table One Name	3
2. Table Two Name.....	8

LIST OF FIGURES

[If list of figures continues to more than one page, the following pages must have a header: LIST OF FIGURES – CONTINUED and include Figure and Page titles.]

Figure	Page
1. Figure One Name	3
2. Figure Two Name	8

[GLOSSARY or NOMENCLATURE, optional]

ABSTRACT

To improve physics models of the solar transition region, the Multi-Order Solar EUV Spectrograph has been built by a team led by Dr. Charles Kankelborg to perform imaging spectroscopy of the sun at EUV wavelengths. Launched first in 2006, the instrument performed simultaneous imaging and spectroscopy over a narrow band centered around 30.4 nm. The amount of science that can be accomplished with the instrument is limited by its bandwidth, which must be small to reduce ambiguity in its data. This limitation can be avoided by launching an array of instruments operating at different wavelengths, piecing together a comprehensive view of transition region activity on a wide bandwidth. However, the command and data handling (C&DH) system on the current MOSES payload cannot support multiple instruments, and a new system must be built to support the addition of more instrumentation. To this end, designs based on a centralized computer topology and a distributed computer topology have been created for a new C&DH system to support the existing MOSES instrument, an EUV Snapshot Imaging Spectrograph (ESIS) and an improved guide scope. It was found that the frame rate of the entire electro-optical system was limited mostly by the low sensitivity of the optics, and that the mass of the electronics

[Single spaced and no more than 350 words, indent first line five spaces. The abstract must contain the following elements: (1) statement of the problem, (2) procedure or methods, (3) results, and (4) conclusions. Mathematical formulas, abbreviations, diagrams, and other illustrative materials should not be included. It should be written to be understood by a person who does not have expertise in the field.]

INTRODUCTION

Solar Physics and the Multi Order Solar EUV Spectrograph (MOSES)

The sun has been a great source of curiosity for humankind for a long time. It is believed that people first began to study the skies as early as 4000 B.C. (Giorgio, 1952). The history of astronomy can be divided into three periods, the first of which (Ancient Astronomy) extended from 4000 B.C. to 500 A.D. From 500 A.D. to 1500 A.D., Giorgio describes a period of Medieval Astronomy in which there is a lack of progress due to a lag in technological advances and also religious suppression. In 1543, when he published *De Revolutionibus* (Giorgio, 1952), Nicolaus Copernicus's heliocentric view of the universe provided a springboard upon which the rapid progress of the Modern era of astronomy began.

Around the year 1600, several people were simultaneously inventing the telescope (Andersen, 2006). The first patent for a telescope was issued to Hans Leppershey in 1608; however, there were other people working on and publishing information on telescopes as early as 1571. Thomas Digges wrote about a device his father built which used two pieces of glass and allowed him to see at a distance of seven miles "what hath been doon at that instante in private places." (Andersen, 2006). In the centuries since, a growing number of astronomers armed with increasingly powerful optical and spectroscopic devices have had their eyes on the skies.

An ultraviolet spectrometer was launched out of the earth's atmosphere for the first time by Wehrner von Braun in March of 1944 as part of atmospheric measurements intended to aid the Nazi's calculation of rocket trajectories (Seibert, 2006). After being captured by the U.S. during WWII, he was relocated to White Sands, New Mexico where he continued his research on rockets and space exploration. His work pioneered the use of sounding rockets for UV solar observation. In 1973 with the launch of the Apollo Telescope Mount aboard Skylab, another breakthrough development occurred through the experiment SO82 (Rein & Eugene, 1974). Experiment SO82A was a slit-less spectroheliograph, which created the famous "overlappograms", showing multiple images of the sun offset by wavelength in the same frame, as shown in fig. 1 (Rein, et al., 1974).

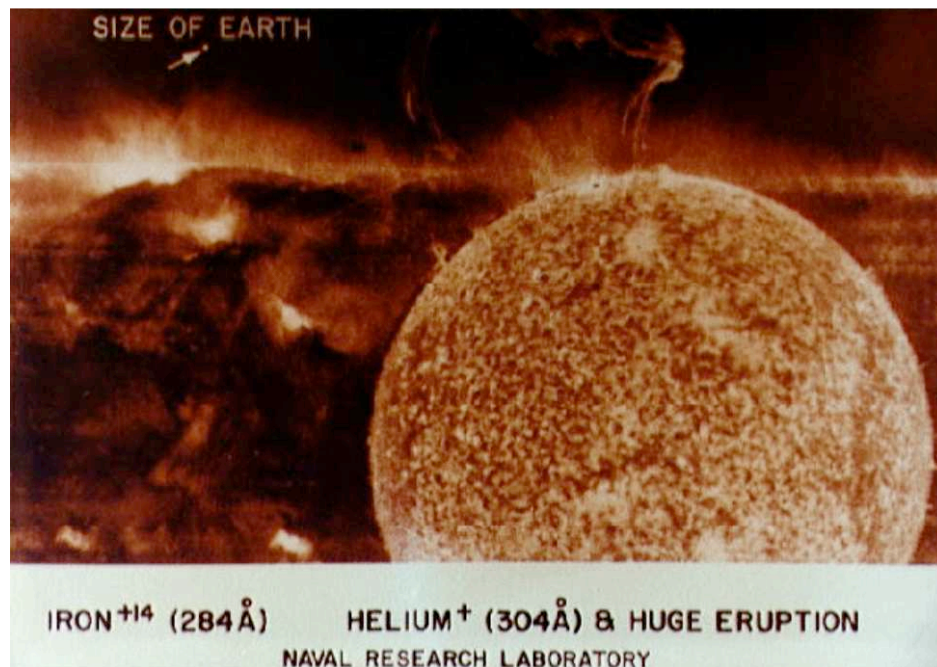


Figure 1: Image From Skylab Experiment SO82A

In 1985, the solar disk was imaged by a group led by J. H. Underwood for the first time at XUV wavelengths with normal incidence optics (Underwood, Bruner, Haisch, Brown, & Acton, 1985). Multilayer coatings were used to enhance the reflectivity and wavelength selectivity of the mirrors used in the telescope. This technology was further refined later with the launches of the Multi-spectral Solar Telescope Array (MSSTA) by Arthur B.C. Walker, Jr. in 1991 (DeForest, 1995), and the Normal Incidence X-ray Telescope (NIXT) by Leon Golub in 1989 (Golub, et al., 1990). In 1988 the Solar EUV Rocket Telescope and Spectrograph (SERTS) was launched by Werner Neupert (Neupert, Epstein, & Thomas, 1992). Using a novel multi-layer-coated grating toroidal mirror, SERTS boasted the capability to take both spectroheliograms and spectrograms using dual-purpose optics. From this long history of scientific struggle and progress, it can be seen that there is a great desire by the solar physics community to observe the solar atmosphere with spectroheliograms and spectrograms at high spatial, spectral and temporal resolution. To this end, a team led by Charles Kankelborg at Montana State University has created MOSES, the Multi-Order Solar EUV Spectrograph (Kankelborg, et al., 2006) (Fox, 2011).

The goal of the MOSES project is to achieve simultaneous imaging and spectroscopy of the sun at 30.4 nm. As can be seen in fig.2, an image from the Solar and Heliospheric Observatory (SOHO), the sun is very active and has numerous large features that can be seen at this wavelength. The optical bandwidth of the MOSES instrument is limited such that it only detects light from two spectral lines, He II (30.38 nm) and Si XI(30.33 nm).

Light from the He II line makes up approximately 90% of the received flux, so the observed spectrum primarily shows Doppler shifts and line broadening caused by the movement of He II features on the sun. The instrument thus effectively produces an image, a velocity map, and a line width map of the surface of the sun, providing an insight to solar activity that was not previously available. Though it has not been attempted, it may also be possible to separate the He II and Si XI lines in the image data and generate distinct spectroheliograms for the two bands.

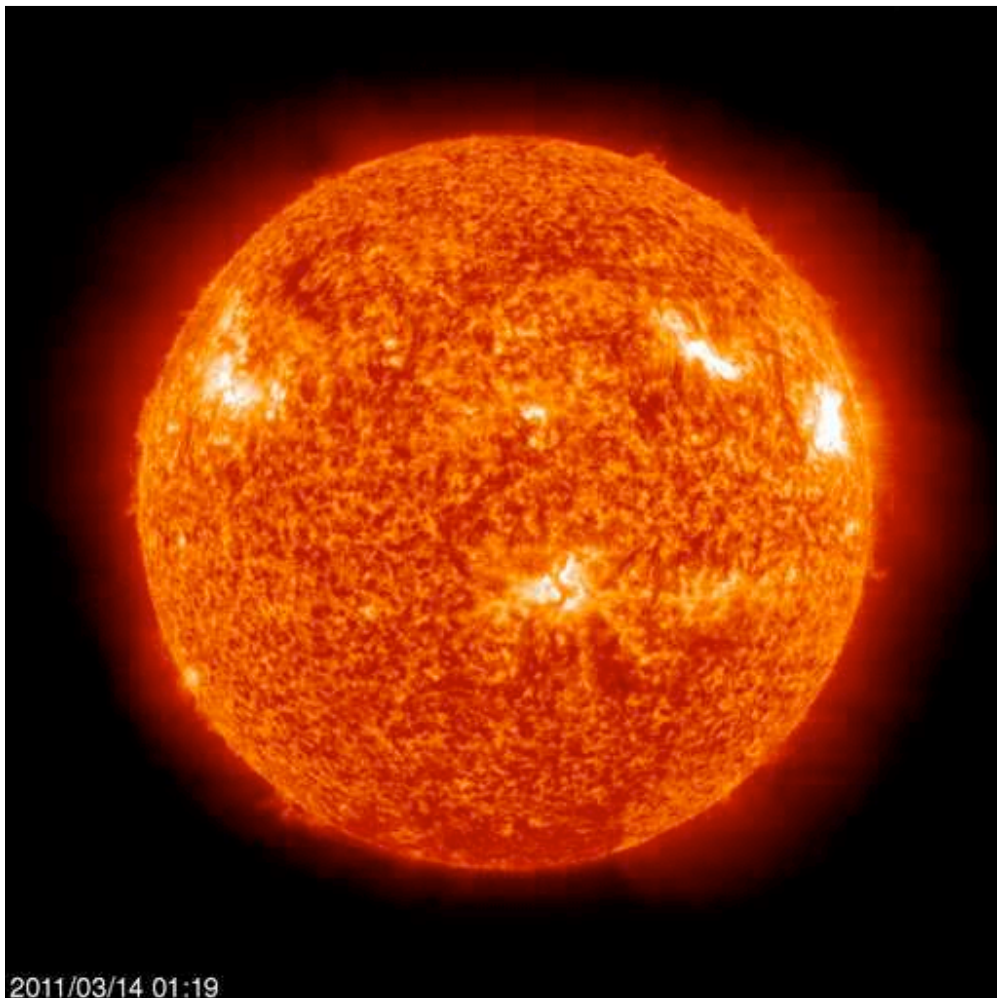


Figure 2: An image from the Extreme Ultraviolet Imaging Telescope (EIT) aboard SOHO at 30.4 nm

Optically, the instrument consists of an aperture, a primary mirror, a secondary mirror, three filters (not shown), and three CCD's, as shown in fig. 3. Light enters through the square aperture and is reflected from the primary mirror (G1) to the secondary mirror (fold flat) and then finally is focused onto the detectors. The primary mirror (G1) is a multilayer-coated concave spherical diffraction grating that is optimized to diffract light entirely into the zeroth and ± 1 spectral orders; the secondary mirror is a multilayer-coated flat. A trio of 1024x2048 pixel CCD's captures the image created by each of the orders of the primary mirror, and sensitive readout electronics provided by Mullard Space Science Laboratory amplify and digitize the generated photoelectrons with a resolution of 14 bits per pixel.

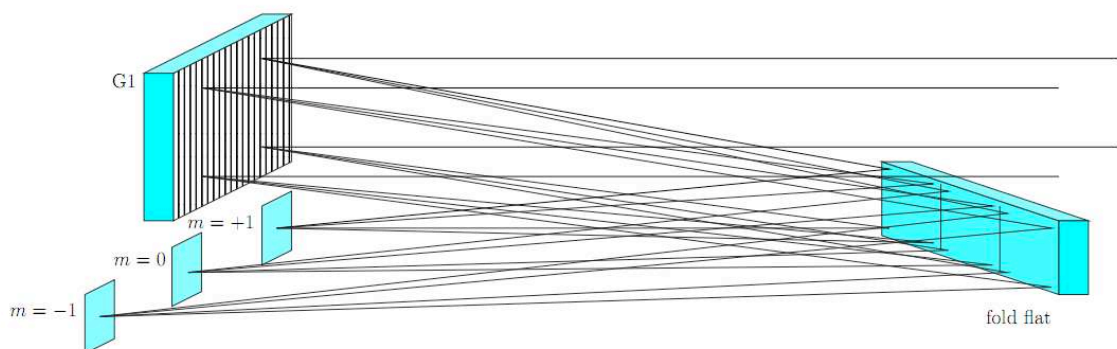


Figure 3: MOSES Instrument Optical Layout (Kankelborg C. , 2006)

The Need to go to Space

One important aspect of this mission is that it cannot be done terrestrially. The optical depth of the atmosphere is 0.41 for light at 30.4 nm observed at an altitude of 225

km, yielding a transmittance of 66% (Hinteregger, 1692). At sea level, the atmosphere is opaque at this wavelength. Therefore, the instrument must be launched beyond the atmosphere if it is to collect appreciable numbers of solar EUV photons.

There are several options for lofting an instrument to high altitudes. One could consider lugging equipment to the top of a high mountain. However, there simply is not a mountain high enough to get beyond the thick blanket of Earth's atmosphere. Mount Everest is only 8.8 km tall, while the apogee of the first flight of MOSES was 263 km. This is beyond the Kármán line, past which an aeronautical vehicle would have to travel faster than orbital velocity to sustain flight. Airplanes are thus ruled out as well. The world record for a gas balloon flight is currently held by the Japanese (Yamagami), who launched a balloon fabricated using a 3.4 μm thin film to an altitude of 53 km. The only two known options that can achieve the required altitude are sounding rockets and satellites.

For a university student project, building a nanosat-class satellite is a realizable goal. This is due in part to the AFRL-sponsored University NanoSat program, a competition in which the Air Force gives universities money to build satellites and compete for launches provided by NASA. The current design for the MOSES instrument makes use of a primary mirror with a 9.8 m focal length, much too long to fit on a nanosat class platform. Therefore, sounding rockets are an attractive option. A sounding rocket payload is a realizable student project, can achieve the desired altitude, and can accommodate much larger payload sizes and weights than a nanosatellite.

Motivation for Command and Data Handling Subsystem Redesign

In 2012, the MOSES payload will be launched with existing instruments that will be retooled to operate at a new wavelength. Thereafter, work will begin on the second generation MOSES payload, which will include both the existing spectroscopic imager and a new instrument. The new instrument will be optically similar to the existing one, but it will operate at a different wavelength and use different detectors. As will be seen later in this chapter, the command and data handling system does not currently have the capability to handle an increased number of instruments without reducing the number of exposures from the current instrument, which is highly undesirable. In this section, the relationship between payload mass, system performance, and observation time will be explored so that design guidelines can be established.

Observation time is dependent on the the mass of the payload. The kinetic energy produced by the rocket engine becomes potential energy as the rocket ascends; therefore the rocket payload can go higher if it has less mass. From the Mission Readiness Review (MRR) (Payne, 2006), the total mass of the MOSES payload is 1180.2 lb. and the estimated observation time above 160km is 301.1 s. The mass includes not only the optical table, but also the nose cone, the boost guidance system, two telemetry sections, the parachute, and the Solar Pointing Attitude Rocket Control System (SPARCS). When fully skinned up, the experiment section of the MOSES payload weighs approximately 400 lb.

The amount of observation time can be calculated by finding twice the time it takes for a point mass with the same mass as the payload to fall from apogee to the minimum observation altitude, 160km. This can be calculated using equation 1, (Kankelborg & Fox, 2011):

$$T = 2 \sqrt{\frac{R_e + H_a}{2gR_e^2}} \left[\sqrt{(R_e + H_o)(H_a - H_o)} + (R_e + H_a) \cos^{-1} \sqrt{\frac{R_e + H_o}{R_e + H_a}} \right] \text{ Seconds} \quad \text{Eq. 1}$$

Where

T = Observation time

g = Acceleration due to gravity at sea level (9.81 m s^{-2})

H_a = Apogee altitude

H_o =Minimum observation altitude

R_e = Radius of the Earth

Finding the apogee altitude from first principles is beyond the scope of this paper, and it can change due to events outside of our control. Furthermore, the final configuration of the rocket may include ballast that is used to move the center of gravity so that the rocket is stable under power. Also, the thrust provided by the rocket engines can vary due to slight variances in manufacturing. Finally, the aerodynamic drag encountered by the rocket will vary with atmospheric conditions. All this uncertainty is dealt with by specifying also the 2- σ observation time, which is two standard deviations lower than the

average time. For the original MOSES flight, this was 283 seconds, 6% lower than the nominal observation time (Payne, 2006). The actual observation time of the 2006 MOSES flight was 296 seconds and the apogee was 262,840 m (Fox, 2011), but the time above 160km was 301.1 s to within half a second.

In figure 4, a graph that was reproduced from the sounding rocket program handbook (Sounding Rocket Program Office, 2001) shows the estimated apogee for a collection of different payload masses. This graph does not agree with the data in the MRR, possibly because there is extra drag on our payload since it has a larger diameter than the rocket body. Data points for apogee altitude vs. mass at a launch angle of 87° were read from the graph and a quadratic fit was done. The resulting equation is:

$$H_a = 0.294m^2 - 864.7m + 903,900 \text{ km} \quad \text{Eq. 2}$$

Where m is the payload mass in kilograms.

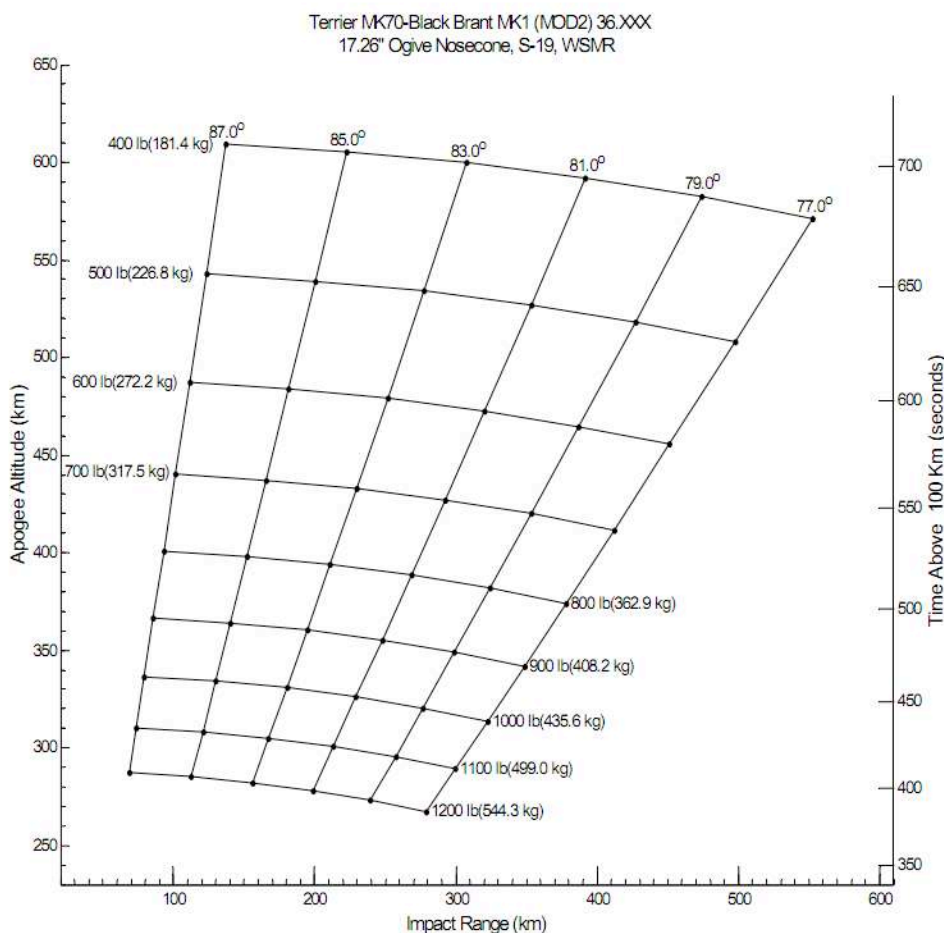


Figure 4: Apogee vs. Weight and Launch Angle (Sounding Rocket Program Office, 2001)

Equation 2 still doesn't describe the MOSES payload- instead, it describes some standard payload that NASA used to generate the graph above. In the MRR, there are two trajectories specified for the MOSES mission. One is for the payload that actually flew, weighing 1180.2 lb, launched at an angle of 86.3°, and reaching apogee at 262.9 km. The second is for a version without the extra telemetry section, weighing 1046.3 lb, launched at an angle of 86.6°, and reaching apogee at 277.2 km. The document doesn't list specifically what the differences between the two configurations are- the 1046 lb

configuration was not flown and full documentation was not provided. The T-610S transmitter from L3Com that was used is also no longer in production. However, the combined weight of a similar T-709 transmitter (7 lb), a pack of C cells required to run it (6 lb) and the 17" microstrip antenna it requires (less than a pound) make up only a small fraction of the 134 lb difference between the two configurations, so the difference must largely be due to the extra structure required to hold the hardware. The 1180 lb version was 28" longer than the 1046 lb version. It is likely that the configuration used will be different than that of either version presented in the MRR, so the uncertainty in the amount of mass lost by removing a transmitter is likely much bigger than the mass of the transmitter itself. Figure 5 shows two sets of apogee and mass data with two curve fits that were generated using the data. The diamond shaped markers in figure 5 represent data points for apogee vs. payload mass that were taken from the chart in figure 4. The squares represent the curve fit that was described earlier with equation 2, and the triangles are the two data points provided in the MRR.

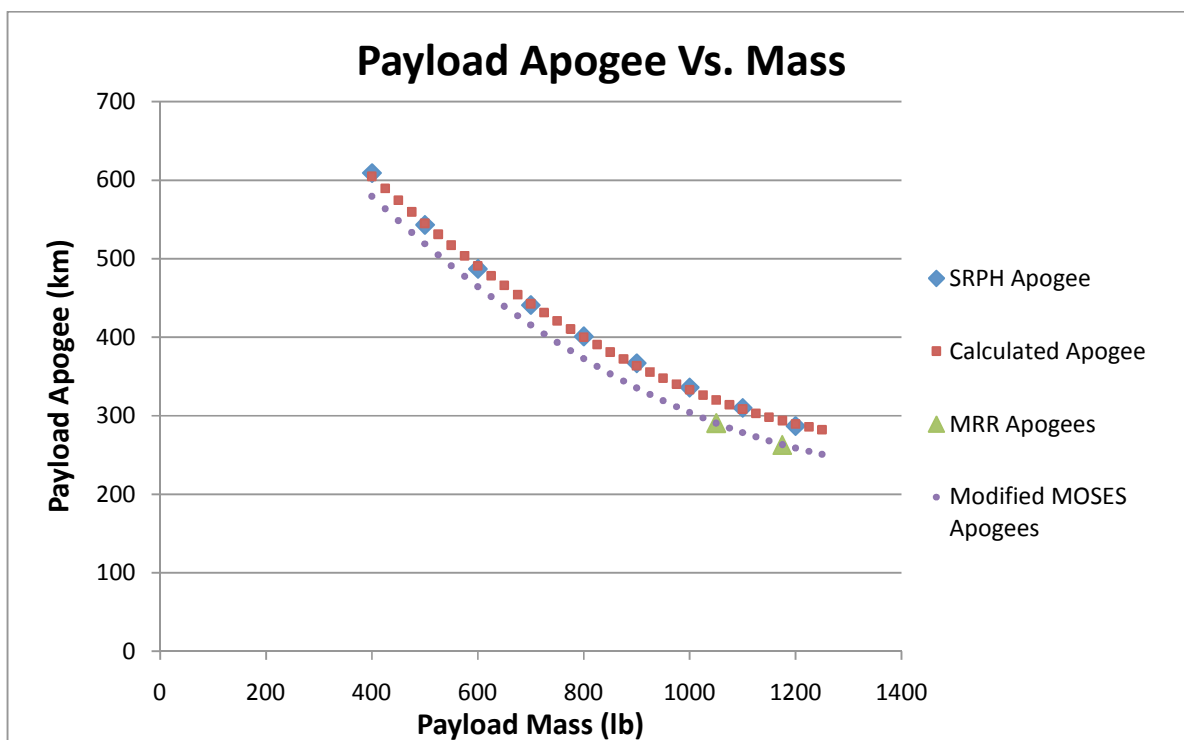


Figure 5: Payload Apogee vs. Mass

The data set represented with circles in figure 5 was generated using equation 3. The offset and the first order term in equation 2 were arbitrarily adjusted to fit the two data points in the provided in the MRR. The shape of the curve was found using data from the Sounding Rocket Program Handbook and it was translated to fit the data in the MRR.

$$H_a = 0.294m^2 - 860m + 868,800 \text{ km} \quad \text{Eq. 3}$$

For payload masses within a range of 900 to 1300 lb, equation 3 should be accurate enough to allow a systems engineer to make design decisions that are affected by payload mass. Using the results from equation 3 in equation 1 table 1, a list of observation times for possible payload masses, was generated.

Table 1: Observation Time Vs. Mass

Payload Mass (Lb)	Observation Time (s)
900	393.4
925	383.7
950	374.3
975	365.1
1000	356.2
1025	347.5
1046	340.8*
1050	339.2
1075	331.2
1100	323.5
1125	316.2
1150	309.3
1175	302.8
1182	301.1*
1200	296.7
1225	291.1
1250	285.9
1275	281.3
1300	277.1

*Data from the MRR (Payne, 2006) for comparison with the calculated data.

The 2006 flight configuration of the payload included two transmitters, one of which was used for science data downlink in the event that the payload was destroyed upon reentry. At the expense of some reliability, the mass of the payload could be reduced to 1046 lb by removing the extra telemetry unit, which would result in a gain of 39.7 seconds of observation time. The rest of the NASA provided hardware was mission critical, so any remaining weight loss would have to come from removing hardware mounted on the MOSES optical table, which is an unlikely possibility given that the goal is to fly more hardware. The removal of the extra telemetry section frees up 134 lb of mass that could

be used to upgrade optics and electronics for the second generation MOSES payload without reducing observation time. Furthermore, in table 1 it can be seen that the reduction in apogee time vs added mass decreases as more mass is added. If necessary, the payload could expand to 1,225 lb and only lose ten seconds of observation time.

Next the performance of the existing computer system will be examined to see if it is possible to run more instruments using the existing hardware. The MOSES instrument took a series of images on its February 2006 flight with varying exposure lengths. Table 2 (reproduced from a 2009 internal group report with permission from Hans Courier) lists the exposure sequence that was run, including the length of each exposure. The main portion of the-data taking routine consisted of fourteen 3 s exposures, each of which took on average 9.18 s for the camera to complete.

Table 2: 2006 MOSES Launch Exposure Times

Frame #	Start time UT	End time UT	Start time (s)	End time (s)	Error \pm (s)	Exposure Duration (s)
Dark 1						
0	18:05:41.20	18:05:41.45	0.00	0.25	0.05	0.25000
1	18:05:47.55	18:05:48.30	6.35	7.10	0.05	0.75000
2	18:05:54.30	18:05:55.80	13.10	14.60	0.05	1.50000
3	18:06:01.90	18:06:04.96	20.70	23.76	0.05	3.05996
4	18:06:10.95	18:06:16.99	29.75	35.79	0.05	6.03978
5	18:06:23.50	18:06:35.50	42.30	54.30	0.05	12.00000
6	18:06:42.10	18:07:06.10	60.90	84.90	0.10	24.00000
Dark 2						
0	18:45:17.15	18:45:17.40	0.00	0.25	0.05	0.25000
1	18:45:23.15	18:45:45.18	6.00	28.03	0.05	22.02993
Data Default						
0	18:45:54.00	18:45:54.25	0.00	0.25	0.05	0.25000
1	18:46:00.30	18:46:01.05	6.30	7.05	0.05	0.75000
2	18:46:07.00	18:46:08.50	13.00	14.50	0.05	1.50000
3	18:46:14.55	18:46:20.55	20.55	26.55	0.05	6.00000
4	18:46:26.70	18:46:38.70	32.70	44.70	0.05	12.00000
5	18:46:44.95	18:47:08.99	50.95	74.99	0.05	24.03969
6	18:47:15.15	18:47:18.22	81.15	84.22	0.10	3.06981
7	18:47:24.40	18:47:27.48	90.40	93.48	0.10	3.07972
8	18:47:33.65	18:47:36.75	99.65	102.75	0.10	3.09981
9	18:47:42.95	18:47:46.03	108.95	112.03	0.10	3.07982
10	18:47:52.20	18:47:55.27	118.20	121.27	0.10	3.06970
11	18:48:01.45	18:48:04.45	127.45	130.45	0.10	3.00000
12	18:48:10.70	18:48:13.77	136.70	139.77	0.10	3.06974
13	18:48:19.95	18:48:23.04	145.95	149.04	0.10	3.08979
14	18:48:29.20	18:48:32.28	155.20	158.28	0.10	3.07981
16	18:48:47.85	18:48:50.85	173.85	176.85	0.10	3.00000
17	18:48:57.05	18:49:00.14	183.05	186.14	0.10	3.08983
18	18:49:06.30	18:49:09.36	192.30	195.36	0.10	3.05984
19	18:49:15.50	18:49:18.58	201.50	204.58	0.10	3.07980
20	18:49:24.75	18:49:27.84	210.75	213.84	0.10	3.08983
21	18:49:34.10	18:49:58.19	220.10	244.19	0.10	24.08973
22	18:50:04.35	18:50:16.35	250.35	262.35	0.10	12.00000
23	18:50:22.65	18:50:28.65	268.65	274.65	0.10	6.00000
24	18:50:35.00	18:50:36.56	281.00	282.56	0.10	1.55980
25	18:50:42.75	18:50:43.50	288.75	289.50	0.10	0.75000

Frame #	Start time UT	End time UT	Start time (s)	End time (s)	Error ±(s)	Exposure Duration (s)
26	18:50:49.70	18:50:49.95	295.70	295.95	0.10	0.25000
Dark 3						
0	18:51:04.15	18:51:04.40	0.00	0.25	0.05	0.25000
1	18:51:10.20	18:51:22.24	6.05	18.09	0.05	12.03986
Dark 4						
0	18:51:30.10	18:51:30.35	0.00	0.25	0.05	0.25000
1	18:51:36.15	18:51:36.90	6.05	6.80	0.05	0.75015
2	18:51:42.70	18:51:44.20	12.60	14.10	0.05	1.50000
3	18:51:50.00	18:51:53.00	19.90	22.90	0.05	3.00000

Each exposure cycle includes three sections: exposing the CCD, reading out the CCD, and storing the data to a disk drive. The 3 s exposure time was chosen based on an end-to-end radiometric calibration of MOSES done at Rutherford Appleton Laboratory (Kankelborg C. , 2006). For the purpose of this paper this is unchangeable, since it would require altering the optical design which is beyond the scope of this study. The CCD readout time is determined by the product of the number of pixels and the pixel clock rate of the readout electronics. According to documentation on the readout electronics provided by the Mullard Space Science Laboratory (Thomas, 2004), the clock rate is set to 2 MHz. The read out electronics (ROE) sample 1024x2048 pixels for each CCD, and they read out four CCD's. There isn't a fourth CCD, but the ROE still goes through the motions of attempting to read it out, because it is a four-channel system. Thus, it nominally takes 4.2 s to complete the read-out cycle. However, the date link protocol used by the ROE incorporates periods of silence, an overhead which extends the readout time to 4.5 seconds.

The remaining 1.68 s from the 9.18 s exposure cycle was spent writing image data to the disk drive, reading instrument state of health sensors (temperature, current, voltage, etc.), sending and receiving telemetry. The disk drive used during the first flight of MOSES was a BitMicro 2A33 one gigabyte solid state drive with a sustained write speed of 14 MB/s. Thus, 0.9 s of processor time from each exposure cycle was used to write each 12.6 MB image set to the disk drive, and 0.78 seconds was used for general instrument operation. As the rest of the exposure cycle is taken up with real-time tasks, the 0.78 second period at the end is the only portion which could be reduced by software optimization to free up time to operate a second instrument. Even with extensive software optimization, it can be seen that there is not enough processor time available to operate a second instrument, and it is necessary to design a new system for a multiple instrument payload.

Thesis Overview

This paper will present two approaches for implementing an improved command and data handling (C&DH) system for the MOSES payload. One will consist of a single, powerful computer, which will store data from all the cameras in the payload, and the second will be a network of smaller computers, each storing data from one camera. First, the paper will examine C&DH system designs from two previous sounding rocket missions, MSSTA II, and the first launch of MOSES, in an attempt to find the aspects of the two designs which allowed the MSSTA to carry 19 instruments and those which imposed

difficulties and delays on the first flight of MOSES. Armed with a set of design principles, a suite of cameras will be chosen and two computer designs will be synthesized, one of which will be a centralized design, and the other distributed. A set of design metrics will be defined and used to compare the two designs, and design guidelines will be created to aid in the future redesign of the MOSES payload command and data handling system.

PREVIOUS DESIGNS

Introduction

To achieve the goal of adding more instrumentation to the MOSES payload, it is helpful to look at designs that were successful in the past and use lessons learned from history to guide decisions in the present. In particular, the design of the Multi-Spectral Solar Telescope Array (MSSTA) promises to yield helpful guidelines (Kankelborg C. C., 1996) (DeForest, 1995). On its second flight, 19 instruments were used capture radiation at 14 different wavelengths. This section of the paper will discuss the attributes of MSSTA that facilitated this feat. Also, this section will look back to the first flight of MOSES in order to find those attributes of the system that could be changed to improve the ease with which more instruments could be added.

MSSTA II

Designed by a research group led by Arthur B. C. Walker at Stanford and launched for the first time in May of 1991, MSSTA used a large array of telescopes with normal-incidence optics to create spectroheliograms of the sun in several EUV/XUV bandpasses. During the second flight of MSSTA in November of 1994, 19 instruments captured images with 16 cameras at 14 different wavelengths (Martinez-Galarce, et al., 2000). The

group was able to launch MSSTA in 1991 with 14 instruments, in 1994 with 19 instruments, and in 2002 with 11 instruments. This rapid series of launches with large instrument manifests indicates that there are lessons to be learned from the design of MSSTA.

The array of cameras, which were all based on the Pentax 645 70 mm camera body, was controlled with two microcontrollers (MCU) that were programmed in assembly and used no operating system (Kankelborg, 1996). These two processors were in turn commanded by a third microcontroller board over a serial network referred to as the Birdnet (Kankelborg C. C., 1996). Each of the camera control boards had interfaces for eight cameras, and the system was expandable- more camera control boards could be added if necessary. This was facilitated by the simple, low-bandwidth nature of the interface between the cameras and the computer, which consisted of shutter switches, motor controls, supply current and voltage sensors. In contrast, the interface between the CCDs on the MOSES spectroscopic imager and its flight computer is a winding path leading from the read out electronics (ROE), through a deserializer, into an FPGA and finally into the computer's PCI bus. The mass of the electronics and the power required to run them has increased with the use of CCDs, despite large advances in technology. In the race towards higher-resolution CCD's, some of the simplicity of film cameras has been lost, raising the question, what are the desirable aspects of film over CCD and CMOS detectors?

There are at least three advantages that film has over the current selection of CCD and CMOS detectors in the application of a sounding rocket mission. These include standardized detector formats, simple electrical interfaces, and the ability to do all data handling post-flight. To begin with, during the second flight of MSSTA, all instruments used cameras based on the Pentax 645 70 mm camera body (Kankelborg C. , 2010). However, due to differing requirements among the collection of instruments, some of the cameras were loaded with different films. In fact, there were multiples types of EUV sensitive film available in the 70 mm format, including Kodak XUV100, Kodak Spectrographic 649, Agfa 10E56, and Kodak Technical Pan, among others. With no modification to flight hardware the “sensor” could be changed, altering the spectral response, sensitivity, and resolution of the instrument. Since the same camera body could be used with different detectors, the mechanical and electrical interfaces for each instrument were identical. This saved the MSSTA group much time and effort in implementing their design. A second benefit of using a film-based system is that the electrical interface between the camera and the C&DH systems can be much simpler than with a solid state detector. In the simplest case, a single GPIO pin could be used to trigger the shutter, assuming the camera automatically advanced the film. However, a solid state detector requires a high speed digital interface such as USB 2.0, LVDS, Firewire, Spacewire, CameraLink, or GigeVision to transfer data between the camera and the storage media. This can increase the amount of time and money needed for software and hardware engineering drastically.

The last benefit of film cameras to be considered is the complete lack of science data handling onboard the rocket payload. After film is exposed, the camera advanced to the next frame and stored the exposed frame in a light proof container. Once on the ground, the film was extracted and developed in a dark room. At no point while the rocket was in the air was any attempt made to read data from the EUV-sensitive media or to handle any data. Contrarily, a solid state detector must be read out and flushed of any residual photocurrent between exposures. This is analogous to implementing an automatic film development process onboard the rocket. While an automatic film development process was implemented on the Soviet satellite Luna -3 (NASA), the images proved to be of low quality and the telemetry system was only quick enough to scan and downlink 17 of the 29 images that were taken before the satellite burned up in the atmosphere. The requirement to read out and flush solid state detectors between exposures necessitates the high bandwidth digital interface to the C&DH system. This increases the minimum required clock speed for the entire system, which then increases the power consumption and thus the mass of the heatsinks and batteries. Also, it can take significantly more time to read out a CCD than it does to advance film by one frame. According to the owner's manual, the Pentax 645 can take ~ 1.5 frames per second with an unspecified exposure time in continuous shooting mode, whereas the MOSES instrument can only achieve 0.147 frames per second per detector with each of its three detectors using a 0.25 second exposure time.

Solid state detectors are, however, clearly the option of choice for future EUV solar observations. In appendix A of his 1995 Ph.D. dissertation, Craig DeForest writes that

development processes used on film from MSSTA had variable results and that there was difficulty maintaining enough process control. Also, all film has a nonlinear radiometric response. These effects lead to a large uncertainty in the accuracy of radiometric measurements. Most importantly, the sensitivity of film was also substantially lower than that of the CCD's used in the MOSES instrument. Figure 6 shows the resulting density of photographic grains for a given number of incident EUV photons per square centimeter at a variety of wavelengths including 33.5 nm.

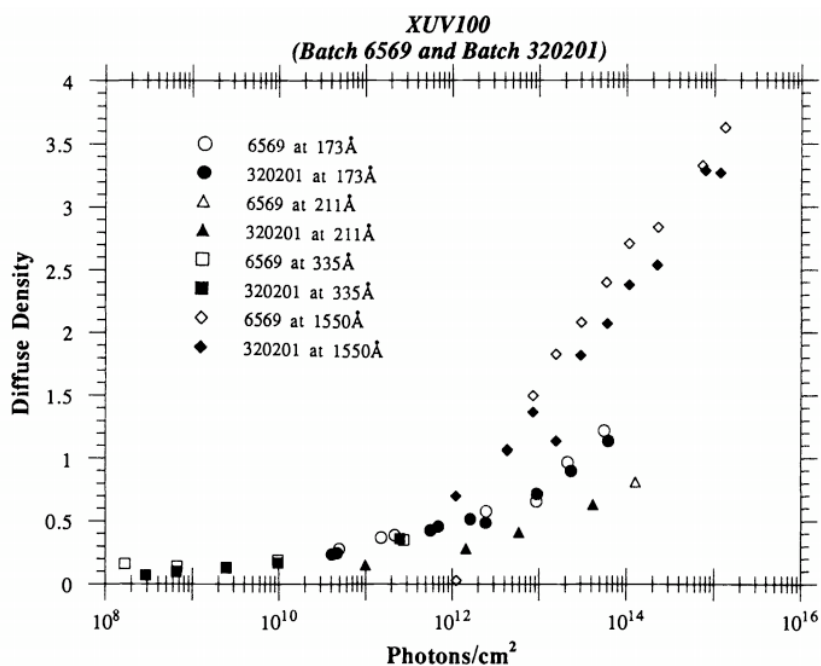


Figure 6: Photographic Response of EUV sensitive film used in MSSTA (Hoover, Walker, DeForest, Allen, & Lindblom, 1991)

The data for the 33.5 nm wavelength stops above a density of 0.5, but it can be seen that sensitivity curve starts to enter the linear region around 10^{12} photons / cm^2 . To compare this sensitivity with that of the CCDs from the MOSES instrument, the lower bound on

their sensitivity (limited by electrical noise) will be found. The MOSES CCD's have a readout noise of approximately 10 electrons per pixel. Coincidentally, an incident photon generates 10 photoelectrons, so the system has a signal-to-noise ratio of one with an illumination of one photon per pixel. The pixels are $13.8 \mu\text{m}$ square, with a fill factor of 100% and a conservatively estimated quantum efficiency of 50%, so this indicates that the lower limit of the CCDs' dynamic range is approximately 1×10^6 photons. This is six orders of magnitude more sensitive than what was possible with film.

A further problem with the use of film is that it does not withstand vacuum very well. The emulsion can crack, and static electricity generated during film transport can expose the film (DeForest, 1995). Dust spots, cracks, and spots generated by static electricity can be removed using software after the film is digitized. Software cannot perfectly remove the spots and scratches, but it can reduce them quite substantially (Kankelborg C. C., 1996).

MOSES

The MOSES payload flown in 2006 carried two instruments. These were the multi-order EUV spectrograph and an H- α guide scope. This section will focus on the MOSES instrument, as data from the H- α telescope is telemetered directly to the ground, bypassing the C&DH system altogether. From an electrical standpoint, the multi-order EUV spectrograph consists of three E2V CCD42-20 charge-coupled devices, specially modified for operation in the EUV and provided to the MOSES group by the team that

built the HINODE EIS instrument (Culhane, Doschek, Watanabe, & Lang, 2002) (Kankelborg C. , 2006), connected to a set of readout electronics (ROE) provided by the Mullard Space Science Laboratory (MSSL). The ROE output is an LVDS port that delivers data at a rate of 32 Mbps. The ROE's LVDS output was connected to a serial-to-parallel converter, which de-serialized the incoming data and output it on a 16 bit parallel bus. This was connected to a PC/104 FPGA module purchased from RPA electronic solutions, Inc., which was installed in the flight computer PC/104 stack. A block diagram of the arrangement is shown in figure 7.

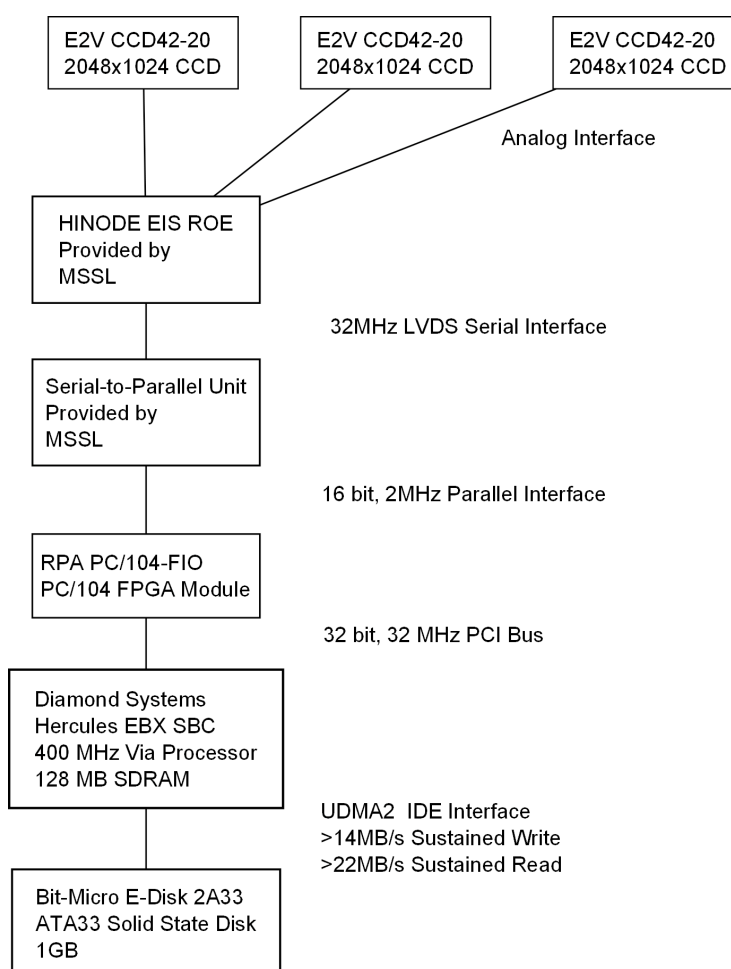


Figure 7: MOSES Instrument Data Path

The flight computer, an EBX form factor single board computer manufactured by Diamond Systems, runs a minimal version of Linux and is connected as shown in the figure to a one gigabyte solid state drive using an ATA33 interface. An important consideration is that there is no data buffering, and a real time operating system was not used. To avoid losing data, the flight software runs at 100% CPU usage continuously to minimize the odds of data loss. Although it uses processor time inefficiently, the software implements a soft real-time system by monopolizing CPU cycles.

During the 2006 flight of the MOSES payload, the activity of the flight computer was inferred using measurements of the ROE supply current. Figure 8 shows a section of a strip chart from the launch with ROE power supply current data on it. Each section of the exposure cycle is labeled. Each dot in the series of horizontal lines on the strip chart represents 100 ms, and ROE supply current is on the vertical axis in units of 100 mA per major tick.

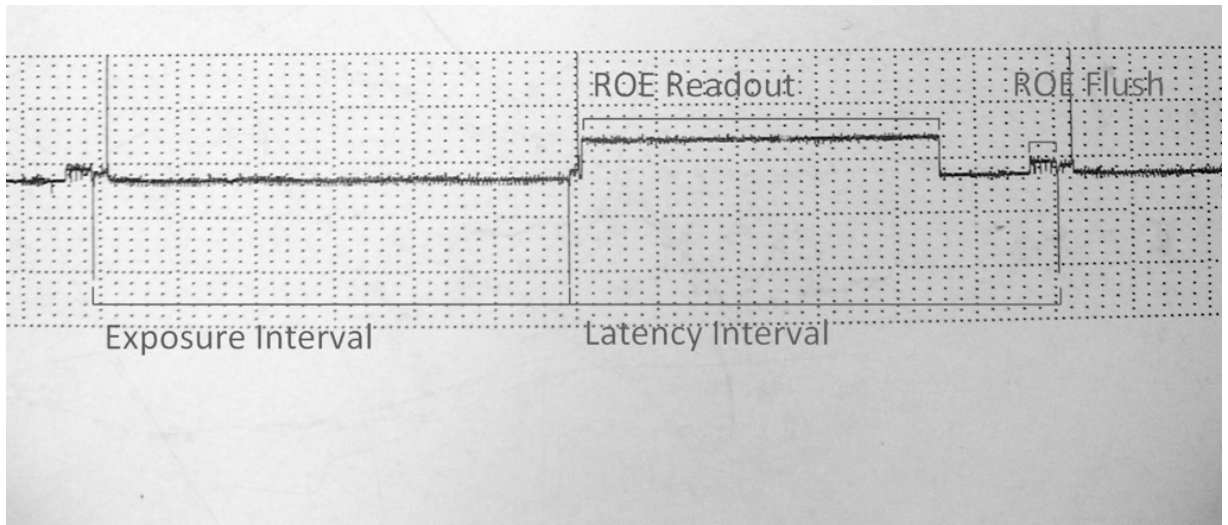


Figure 8: ROE Supply Current Strip Chart

(Reproduced from an internal group report by Hans Courier)

The chart in fig. 8 describes an exposure that was approximately six seconds long. The read-out cycle took approximately 4.5 seconds to complete, which was followed by a 1 second period where the computer wrote the image to disk. Finishing the cycle, the ROE flushed the CCD to prepare for the next exposure. The total latency interval was approximately 6 s long.

It can be seen that the nonstandard LVDS interface used by the ROE complicates the design of the MOSES C&DH system substantially. Input ports typically available on a computer with the bandwidth required to interface with the ROE include Ethernet, USB, PCI, and PCIe. The fact that the data crosses a clock boundary and also must be packetized to interface with those ports means that extra logic in the form of an FPGA or a second processor is required. This introduces extra complexity to the payload design

and increases the mass, power dissipation, and engineering effort required to build the system, all of which are undesirable.

Comparing the designs of MSSTA and MOSES, it is apparent that the careful selection of cameras used in a multiple-detector instrument can facilitate the design process. A system which successfully integrates the superb imaging capabilities of solid state detectors with the simple, modular characteristics of film-based systems could accelerate the development of multi-detector sounding rocket payloads and enable more science to be done. This can be accomplished by using standardized electrical interfaces that are either buffered or DMA or interrupt driven. This will reduce the need for real-time C&DH system operation, allowing it to multi-task. To maximize data output from a multi-detector system, multi-tasking will be essential.

A second lesson to be learned from MSSTA is to use a homogeneous array of detectors. Using the same Pentax 645 camera body for all of the instruments undoubtedly saved a substantial amount of engineering effort during the design of MSSTA. Using solid state detectors, it is unfortunately not yet possible to use different detectors in the same camera body as was done in the days of film; there is no industry standard CCD interface. However, if it can be arranged for all the instruments to use a single interface such as CameraLink or GigeVision, a lot of electrical and software engineering time can be saved. Reducing the amount of software and hardware development will directly reduce the time to launch.

CENTRALIZED VS. DISTRIBUTED COMPUTING TESTBED

In the previous chapter of the thesis, desirable attributes of cameras in multi-instrument payloads were established. In the following section, they will be used to choose a selection of cameras for a hypothetical second flight of MOSES. With a set of cameras in hand, two computer system designs will be synthesized. One will funnel data through a central computer to a single disk drive, and the second will use an array of small, low power computers to store data in a collection of disk drives. The last chapter will then compare the two designs, and give some insight into which topology best fulfills the needs of a multi-instrument sounding rocket payload. The scope of this study will include the computer and any expansion cards that are connected to it, the cooling system, and the batteries required to power the system.

Camera Suite

A scientific objective for the second iteration of the MOSES instrument is to obtain spectra and spectroheliograms in multiple bandpasses. To avoid generating ambiguous “overlappograms” such as those produced by the Skylab SO82A instrument, the optical bandwidth of the MOSES instrument is very narrow. Scientific curiosity is, however, wideband. By launching an array of multi-order spectrographs operating at different wavelengths, this limitation can be overcome. To accomplish this goal, a camera suite consisting of two multi-order spectrographs (the MOSES instrument and ESIS, the EUV Snapshot Imaging Spectrograph) has been chosen. ESIS is currently envisioned as a Gregorian telescope with five spectral orders. The extra information from the two extra

spectral orders will even further reduce ambiguity in the data. It is also desired to replace the original NTSC 648x486 pixel H- α scope with a higher contrast EUV guide scope.

For ESIS and the guide scope, an array of Intevac Microvista cameras (fig. 9) was chosen. These cameras feature back illuminated CMOS detectors designed for UV applications. In table 3, specifications for four candidate cameras are shown. While there may be other cameras that could work for this application, these provide a glimpse into what is available. It is important to note that none have been tested at EUV wavelengths and all would require customization to fulfill the needs of this application.



Figure 9: Intevac Microvista CMOS Camera

Table 3: A Selection of Cameras with Back Illuminated Detectors

Camera	Sensor	Dynamic Range	Resolution (Pixels)	Pixel Size (μm)	Quantum Efficiency at 300nm	Maximum Frames Per Second	Interface
Intevac Microvista	Back Illuminated CMOS	62.5 dB	1280x1024	10.8	~35%	30 ¹	Cameralink Base
Alta U42-UV	Back Illuminated CCD	81.7 dB	2048x2048	13.5	~63% ²	0.4723 ³	Cameralink Base
Fairchild Imaging-Peregrine 486	Back Illuminated CCD	78.42 dB	4096x4097	15	~65%	0.17 ⁴	USB 2.0
JAI CM-140MCL-UV	Back Illuminated CCD	Not Specified	1392x1040	4.65	~50%	16.14 ⁵	Cameralink Base

¹ - At 1280x1024. CMOS devices can operate faster at lower resolutions.

² - UV Enhanced CCD Variant

³ - At 20mS exposure, 2MHz pixel clock.

⁴ - At 20mS exposure, 4MHz pixel clock. (The actual frequency is 1MHz, but there are 4 ports.)

⁵ - At 18mS exposure, 33.75MHz Pixel clock.

The table shows that there is a tradeoff between frame rate and image quality. Both cameras with high frame rates had significantly less dynamic range, resolution, and quantum efficiency than their slower counterparts. The choice between speed and image quality will have to be made based upon science requirements, which aren't yet finalized. In table 4, the data rate for each camera at its maximum frame rate is shown.

Unsurprisingly, the fast cameras generate a lot more data. A system design based on Intevac Microvista cameras will result in a conservative design with a maximum degree of flexibility.

One important feature that the Microvista camera offers as a CMOS device is a rolling shutter. Each pixel can be flushed, exposed, and read out individually, so the exposure

and readout process can occur simultaneously. The Microvista offers a second readout mode, referred to as “pseudo snapshot” mode. In this mode, the pixels are set to expose in a process that takes one readout period (0.033 s). Then the system waits for the exposure duration, and reads out the pixels. A sequence of exposures takes the sum of the lengths of the exposures plus one readout period to complete. This mode is optimal for ESIS because it is necessary to have all the pixels in the image synchronized in time as much as possible. This camera in its stock configuration does not support exposure times longer than 270 ms in pseudo snapshot mode, but it will support 6 s exposures in rolling shutter mode. This study will assume that the manufacturer can provide a customized model that supports 1 s exposures in pseudo snapshot mode that is otherwise identical to the stock model.

Table 4: Camera Data Rates

Camera	Peak data rate	Average data rate at nominal FPS
Intevac Microvista	393.2 Mbps	13.11 Mbps (1 fps)
Alta-U42-UV	23.77 Mbps	23.77 Mbps (0.47 fps)
Fairchild Imaging-Peregrine 486	45.65 Mbps	45.65 Mbps (0.17 fps)
JAI CM-140MCL-UV	233.7 Mbps	14.48 Mbps (1 fps)

Note: 1Mbps= 10^6 bits/sec

For the guide scope, a design based on the Intevac Microvista especially makes sense given the flexibility that it offers as a CMOS device. It can be read out at a variety of resolutions ranging from 1280x1024 to 128x128, at frame rates exceeding 30 frames per

second. This provides flexibility to downlink guide scope video at a resolution, frame rate, and bandwidth of our choosing, without having to perform signal processing in flight to scale the image.

Table 5 shows a proposed camera suite for the second-generation MOSES payload. It includes the original MOSES instrument and the ESIS instrument, designed around the principles of standardization and modularization that were established in chapter two. By choosing the same model of camera for the guide scope and ESIS the mechanical, electrical, and software engineering effort required to build the system is reduced. Hardware and software can be replicated to run any number of identical cameras.

Table 5: Proposed Second Generation MOSES Camera Suite

Instrument	# of Detectors	Manufacturer	Nominal Frame Rate (FPS)	Resolution	Model	Interface
MOSES I Spectroscopic Imager	3	E2v	0.1	2048 x 1024	CCD42-20	16 bit, 2MHz TTL Parallel Interface
ESIS Spectroscopic Imager	5	Intevac	1	1280 x 1024	Microvista	Cameralink Base
Guide Scope	1	Intevac	10	320 x 256	Microvista	Cameralink Base

Note: 1MB = 10⁶ Bytes

Finally, an exposure sequence for the mission must be chosen. With multiple cameras, each camera can take an exposure one at a time in a serial fashion, they could be set to take pictures simultaneously in a parallel fashion, or they could operate independently on their own time scales. In this case, science requirements dictate that each set of detectors

for the spectroscopic imagers operate in parallel, and that the three instruments (the two spectroscopic imagers and the guide scope) be operated independently of each other. It is necessary for the array of detectors making up each of the spectroscopic imagers to expose at the same time so that spectroscopic information encoded in small differences between the images can be extracted accurately.

The frame rate chosen for the new cameras is quite a bit slower than their maximum frame rate, 30 fps. This is because the sensitivity of the new cameras is likely to be similar to that of the current instrument, which took excellent exposures of the EUV sun during its 2006 flight with a 3 s exposure time (Kankelborg C. , 2006). Designing around a slightly faster cadence of 1 fps will allow new instruments to operate slightly faster than the current one, making them able to take advantage of possible improvements in the sensitivity of the optics while not overdesigning the system.

Having chosen a set of cameras and decided how to operate them, the next step is to establish design requirements. A robust, vibration-tolerant and vacuum-compatible mechanical design is a necessity, as well as low power consumption and mass. Functional requirements dictate specifications such as the number of processor cores, their speed, and expansion port bandwidth.

Design Requirements

The C&DH system must perform several functions, which include retrieving and storing data from the camera array, controlling and monitoring the various subsystems of the payload, downlinking instrument status information, and downlinking guide scope video. Table 6 shows a list of the interfaces used by the MOSES I C&DH system, their purpose, and the hardware connected by the interface.

Table 6: MOSES I Computer Interfaces

Interface	Connects From	Connects To	Notes
High Speed Science Data Downlink	CommTech SuperFAST Comm 2-104-ET PC/104+ board	Black Brant IX telemetry systems	Connected to the transmitter baseband input through a filter
MOSES Camera Interface	RPA FIO PC/104+ board	Read Out Electronics (ROE)	16 bit parallel TTL interface clocked at 2MHz
Housekeeping Data Link	Two half-duplex RS422 ports on the Hercules EBX computer	WFF93 PCM encoder stack	1200 baud uplink, 9600 baud downlink
Ethernet Debugging Link	Hercules EBX computer	Ground support equipment	Used for debugging software
Subsystem GPIO	Hercules EBX computer GPIO port	Power control subsystem, WFF93 PCM encoder stack, camera shutter	The motherboard had a 40 pin GPIO interface, 30 pins were used.

The new C&DH system must support the interfaces listed in table 7. For the second-generation MOSES payload, the guide scope video feed has been combined with the housekeeping downlink into one synchronous RS422 link. A second RS422 port would be used for uplinking commands. The camera interfaces were chosen based on the needs of the cameras that were chosen previously. An Ethernet port will still be used for

debugging software. However, in the distributed computing case, a network will have to be built so that ground support equipment can debug all of the computers using just one Ethernet connection. Lastly, 30 lines of TTL GPIO ports were used during the first flight of MOSES. It is likely that this number would increase for the second-generation MOSES payload, but it is not known by how much. For the purpose of this study, it will be assumed that the design will continue to use just 30 GPIO lines.

Table 7: Second-Generation MOSES C&DH System Required Interfaces

Interface	Connects To	Notes
Housekeeping / Guide Scope Data Link	WFF 93 PCM Encoder Synchronous RS 422 Port	1200 baud command uplink, 10 Mbaud downlink
MOSES I Camera Interface	Read Out Electronics (ROE), 16 bit parallel TTL	16 bit parallel TTL interface clocked at 2MHz
ESIS Cameras	5 CameraLink Base Ports	The Intevac Microvista camera requires a pixel clock > 44 MHz.
Guide Scope Camera	1 CameraLink Base Port	The Intevac Microvista camera requires a pixel clock > 44 MHz.
Ethernet Debugging Link	Ground support equipment	Used for debugging software
Subsystem GPIO	30 TTL GPIO Lines	Controls / Monitors subsystems and WFF93 uplinks.

Next, the mechanical requirements of the system will be considered. These are driven largely by the vibration levels that the payload will experience during launch, as well as the goal of having the instrument survive reentry. The primary mission objectives can be completed even if there are large amounts of damage to the payload, provided that the disk drives survive. From table 6.3.4-1 in the Sounding Rocket Program Handbook (Sounding Rocket Program Office, 2001), the payload must survive testing at the vibration levels shown in tables 8 and 9, which should ensure that it will survive the launch intact.

Table 8: Thrust Axis Sine Sweep (Sounding Rocket Program Office, 2001)

Sweep Rate	4 octaves / minute
5-24 Hz	3.84 inches / second
24-110 Hz	1.53 g
110-800 Hz	3.5 g
800- 2000 Hz	10.0 g
Axis	Thrust Axis Only

Table 9: Random Vibration Spectrum, All Axes (Sounding Rocket Program Office, 2001)

Duration	10 seconds / axis
Total Integrated Acceleration	12.7 GRMS
20 Hz	0.01 g ² /Hz Note: 1.8dB /Octave slope between 20Hz and 1000Hz.
1000Hz	0.10 g ² /Hz
1000 – 2000 Hz	0.10 g ² /Hz
Axis	All Axes

These tests are performed with the payload powered up, as it would be during launch.

Most conventional RAM modules used in the popular ATX form factor use card edge

connectors and spring loaded clips to keep the RAM modules seated in the connectors, as is shown in figure 10. In a high vibration environment, the risk that the electrical connections to the RAM could be momentarily broken is too great. Even a short disconnect between RAM and the CPU could lead to a disastrous software crash or a corruption of flight data. Thus, only form factors which use soldered memory will be considered for the MOSES C&DH system.

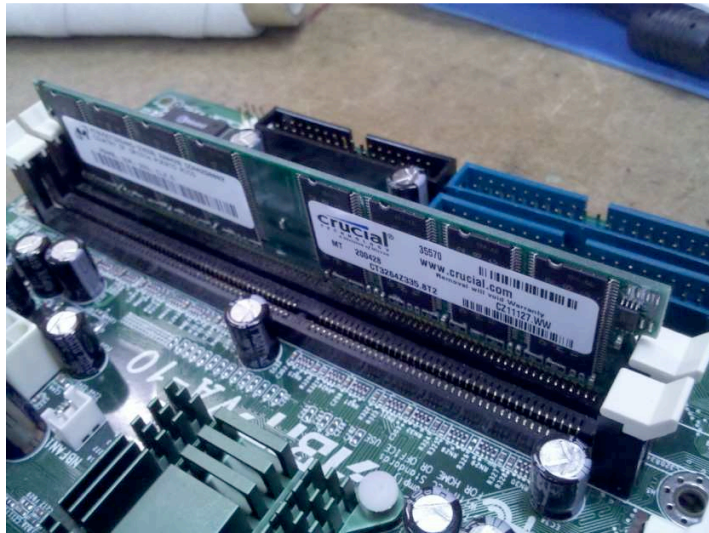


Figure 10: Conventional RAM module with card edge connectors and spring loaded clips

Another important consideration is that the electronics must be conduction cooled. During testing and on the launch rail, the inside of the payload is held in vacuum. EUV optics do not work in the presence of photon-absorbing gas, and it is also necessary to prevent an explosive release of gas when the shutter door is opened in space. On the ground, liquid nitrogen will be plumbed into the payload so that it can be continuously

cooled, and in flight aluminum heat dumps will conduct excess heat from the electronics. In both cases, the convection-based cooling systems typically used on ground-based electronics will not work. With no gas to conduct heat into, the only way a heat sink can lose heat is through black-body radiation. However, the rocket skins will be heated during launch from atmospheric friction, so a highly emissive radiator inside the rocket would receive as much as or more energy than it released. Thus, the heat will be stored using aluminum heat dumps and copper heat pipes, similar to the MOSES I design which is shown in figure 10. In the figure, heat is transported via a series of copper heat pipes from integrated circuits on the left side of the box to the two blocks of aluminum on the right. These were connected to a large aluminum plate underneath the electronics box to a cold finger on the opposite side of the optical table.

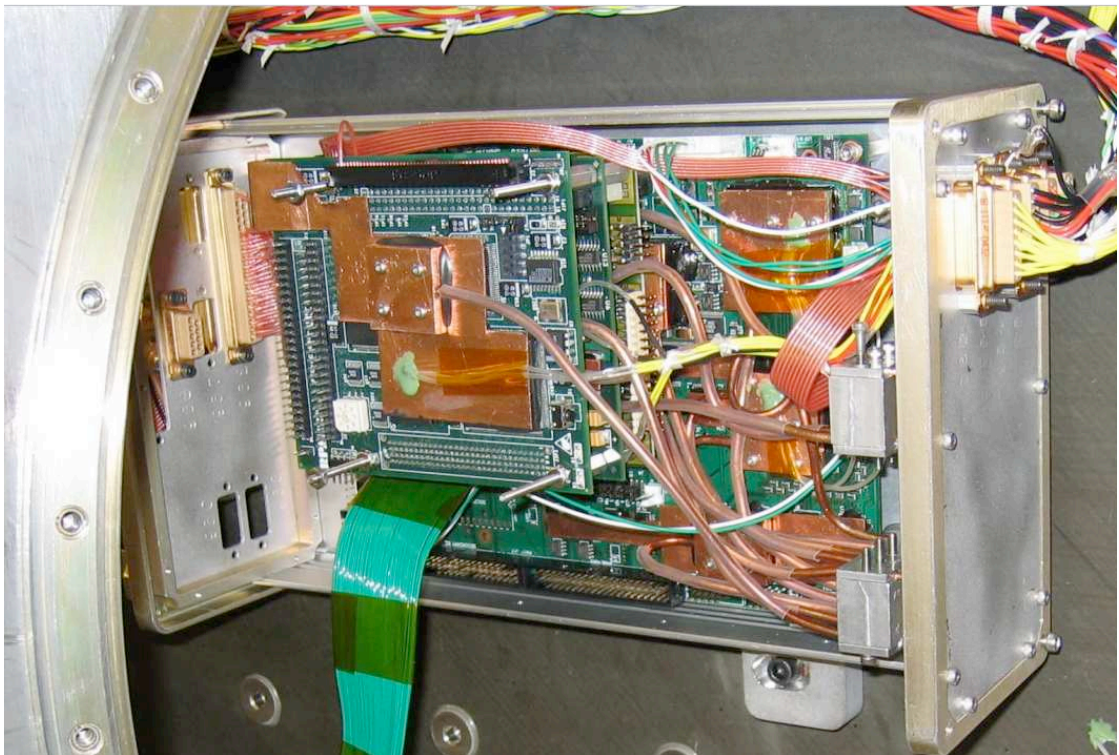


Figure 11: MOSES I Flight Computer

The large number of computer form factors available can be categorized into one of four categories- ATX derivatives, Back planes, stacks, or Computer-on-modules. The first category, ATX derivatives, includes the form factors typically used in consumer computers such as ATX, BTX, MicroATX, Mini-ITX, and so on. ATX based machines are not viable due to a lack of mechanical ruggedness, since they typically use spring loaded card slots for expansion connections. The second category, Computer-on-modules, are small embedded x86 architecture machines such as the GumStix. Computer-on-Modules are also not particularly attractive because they don't typically follow a mechanical interface standard and usually don't have many expansion ports. This leaves back planes and stacked topologies as viable options. Ruggedized, conduction cooled models are available in both topologies, and while back planes may use card edge connectors, they typically use more rugged connectors which maintain a positive lock, ensuring a solid connection. The four types of computer form factors are summarized in table 10.

Table 10: Types of Computer Form Factors

Interconnect Type	Examples	Typical Expansion Interfaces	Soldered RAM Available?	Conduction cooling available?
ATX Derivatives	ATX, MicroATX, BTX, Mini-ITX	PCI, PCIe, Gigabit Ethernet, USB	No	No
Back Planes	VPX, VME, cPCI	PCI, PCIe, Gigabit Ethernet, 10Gigabit Ethernet, RapidIO, Infiniband	Yes	Yes
Stacks	PC/104+,	ISA, PCI, PCIe	Yes	Yes

	PCI/104 Express			
Computer-On-Modules	Gumstix, COMexpress	Non standard	Yes	Yes

As presented by the chart, backplane topologies such as VPX, VME, and cPCI look like attractive options. However, they make use of switched serial fabrics. This is a technology which allows modules to reconfigure themselves and route high-speed data as needed between different modules on the backplane. While it is necessary for some applications, this is not necessary for the MOSES project as all the data connections must be static to ensure reliable operation during flight. It also increases the amount of engineering effort required substantially as a large amount of FPGA development would be necessary to interface with the switched serial fabric.

This leaves stacked topologies such as PC/104, PC/104+, and PC/104 Express. The original PC/104 form factor used the outdated ISA bus, a 16 bit parallel bus that was clocked at 4.77MHz. Using four clock cycles for each transfer, its maximum data rate was 19 Mbps, which is lower than the 32 Mbps data rate that the ROE of the current MOSES instrument outputs. PC/104 is therefore not a valid topology for this application. However, PC/104+ and PC/104 Express are both valid options, supporting the PCI bus and the PCI Express bus, respectively. PC/104+ implements a 32 Bit, 33MHz PCI bus which is shared between all the modules in the stack. With a maximum data rate of 1,067 Mbps, it was the bus of choice for the original MOSES instrument. However, a drawback was that it could only be used by one device at a time, a limitation that can be addressed by using PCI/104 Express instead. The PCI/104 Express standard implements an x16

PCIe bus broken into four separate x1 links and two x4 links. One x4 link is reserved for peripherals built into the motherboard. With a total data rate of 48 Gbps divided into six separate links, PC/104 Express is a good choice for a computer designed to capture data quickly from multiple sources.

Centralized Computing Platform

A design based around one central computer for a multi-instrument payload should be focused on maximizing multi-tasking capability and expansion port bandwidth. With three instruments concurrently producing data, the C&DH system will necessarily have to perform multiple functions and manage large data streams simultaneously. To this end, a system is proposed with a multi-core processor, based on the PC/104 Express topology. The design process will begin by choosing a CPU and determining how much RAM is necessary. This will narrow the range of models to a few that are close to what is needed, and the remaining units will be considered based on how I/O is routed on the motherboard and what peripherals the board has.

First, the number of processor cores necessary to complete the task must be determined. Largely, this is decided by software architecture- how many execution threads need to run to complete the task? One logical way to split up the software would be to have a thread for each instrument and one for command and instrument health reporting purposes. Split this way, a quad-core processor logically would be chosen. However, this is likely a subjective decision that would be made by the software team after the

hardware had already been designed. Therefore, there is no way to determine how many cores are strictly necessary *a priori*. However, it is a common feature built into motherboard BIOS settings to shut down unwanted extra processor cores, so there is no downside to building a computer with as many cores as possible. Unfortunately, embedded technology lags behind consumer technology and dual core processors are just now finding their way onto single-board computers. Since quad core processors are not currently available for the PC/104 Express form factor, a computer using a dual core processor will be chosen. In this case, one possible method of splitting up the software into two threads would be to have one thread managing the Intevac cameras, and another managing the MOSES I instrument and the housekeeping functions.

The processor clock speed is another topic to consider. However, on this subject there are a lot of questions- the software isn't written yet, so its execution time is unknown. Also, the execution time depends on the processor architecture, which is proprietary information. It is known that the first MOSES C&DH system functioned adequately with a 400 MHz CPU clock. Dual core processors are typically available with 1.2 to 3 GHz clock speeds, so the clock speed is not anticipated to be an issue. It is likely that the computer will be deliberately under-clocked during flight to reduce power consumption.

The next task is to determine how much RAM is necessary. This is also largely a function of the software design, but it should be possible to establish a conservative estimate of how much will be needed. The current MOSES system uses a Hercules EBX single board computer purchased from Diamond Systems Corporation, which comes with 128 MB of

RAM soldered to the motherboard. This system currently runs a minimal Linux distribution and the MOSES flight software, which operates the MOSES spectrographic imager and manages all command and instrument-health related functions. With multiple instruments, it might be necessary to implement a data queue in software that merges the data streams, eliminating the chance that data from one instrument could be lost while another is monopolizing the disk drive. Supposing that it was necessary to buffer one second of data in RAM, how much additional RAM would be necessary? For this calculation, a nominal scenario will be assumed: the existing MOSES instrument, the new spectroscopic imager, and the guide scope will all be operating frame rates that would be expected during flight (shown in table 11). The total data rate can be found by multiplying the image size by the number of frames per second and summing for all the instruments. Table 11 shows the average data rate for the proposed instruments.

Table 11: Maximum Average Data Rate for the Proposed Instruments

Instrument	Resolution	Bit Depth	Number of Detectors	Frame Rate	Average Data Rate
MOSES	2048x1024	16 ¹	3	0.1	10.1 Mbps
ESIS	1280x1024	10	5	1	65.5 Mbps
Guide Scope	320x256	10	1	10	8.2 Mbps

¹: The data from the device has 14 bit resolution, and a two-bit CCD ID code is appended.

Converting to bytes per second and summing the three instruments' data rates, the total is 10.4 MB. Of this, 1.0 MB is guide scope data. Since the guide scope is monitored on the ground and used to control the pointing of the instrument, 1 s of latency is undesirable so the amount of buffer used would likely be smaller than 10.4 MB. Adding the buffer size to the previously used 128 MB of RAM, 256 MB of RAM should be sufficient for the

second generation MOSES C&DH system. SDRAM power consumption is proportional to the amount installed (Micron Technology, Inc., 2007) and cannot be turned off in the motherboard BIOS; it is therefore advisable not use more than is necessary. However, a 1GB DDR3 SDRAM module produced by Micron uses less than 0.6 W, 6% of the 10 W that was required to power the first MOSES C&DH system. The risk of not having enough RAM may outweigh the benefits of using a little less power. Furthermore, it is unlikely that a vendor would offer a computer with a dual core processor and only 256 MB of RAM.

The selection of PC/104 Express single board computers with dual core processors is not large. Boards that fit the previously established design parameters are available from Lippert Embedded Computers and RTD Embedded Technologies, Inc. There may also be others. The two computers that were considered, the Lippert GS-45 and the RTD CMA22MVD1860, are very similar machines. Both use Intel Core 2 Duo Processors, and have 1024 MB of soldered RAM onboard. The GS-45 is clocked by default at 2.26 GHz, and the RTD computer runs at 1.8 GHz by default. Both are also available with 1.2 Ghz clock speeds. Specifications listed for the two computer systems and the original MOSES flight computer are shown in table 12. The power consumption of the two boards is very comparable, but it is also two to three times higher than that of the original MOSES C&DH system. Using a smaller form factor, they are both lighter than the original MOSES C&DH system, but the extra mass required to power and cool the two candidates will quickly overshadow the weight loss.

Table 12: Dual Core PCI/104 Express Computer Specifications

Computer	Maximum Power Consumption	Mass	RAM	Clock Frequency Range
Lippert GS-45	32.5 W @ 2.26 GHz	110 g	1024 MB	1.2 – 2.26 GHz
RTD CMA22MVD1860	21 W @ 1.2 GHz 31.5 W @ 1.8 GHz	199 g	1024 MB	1.2- 1.8 GHz
Diamond Systems Hercules EBX	10W @ 550MHz	285 g ¹	128 MB	550 MHz

¹: The Hercules EBX form factor is larger than the PC/104 Express form factor, which is why the mass is higher.

Both computers use the Intel GS-45 embedded chipset with the ICH9M-SFF-Enhanced southbridge and thus have the same basic I/O capabilities, but Lippert and RTD have implemented their designs in subtly different ways, as can be seen in figures 12 and 13. The RTD board is advertised as having eight 1x PCIe ports; however, four of them are routed through a PCIe switch into an x1 port on the ICH (I/O Controller Hub) and must therefore share the bandwidth of an x1 port. Secondly, the RTD board uses a type 2 PCI/104 Express interface, which means that stacking downwards it provides PCIe ports through the PCI/104 Express connector, and stacking upwards it routes PCIe ports, SATA, and USB through the PCI/104 Express connector. The Lippert board, which uses only type 1 PCI/104 Express interfaces, routes only PCIe lanes and USB ports through the PCI/104 Express connector. Standard onboard connectors are used for the SATA ports. Another difference is that the RTD board's two serial ports support RS-422, which will be needed for communication with the WFF93 PCM encoder used to control the system and downlink data. Unfortunately, they are limited to 115.2 Kbps, where this

application requires 8.2 Mbps of throughput to downlink guide scope video. A high-speed RS-422 card would still need to be installed in the PC/104 Express stack.

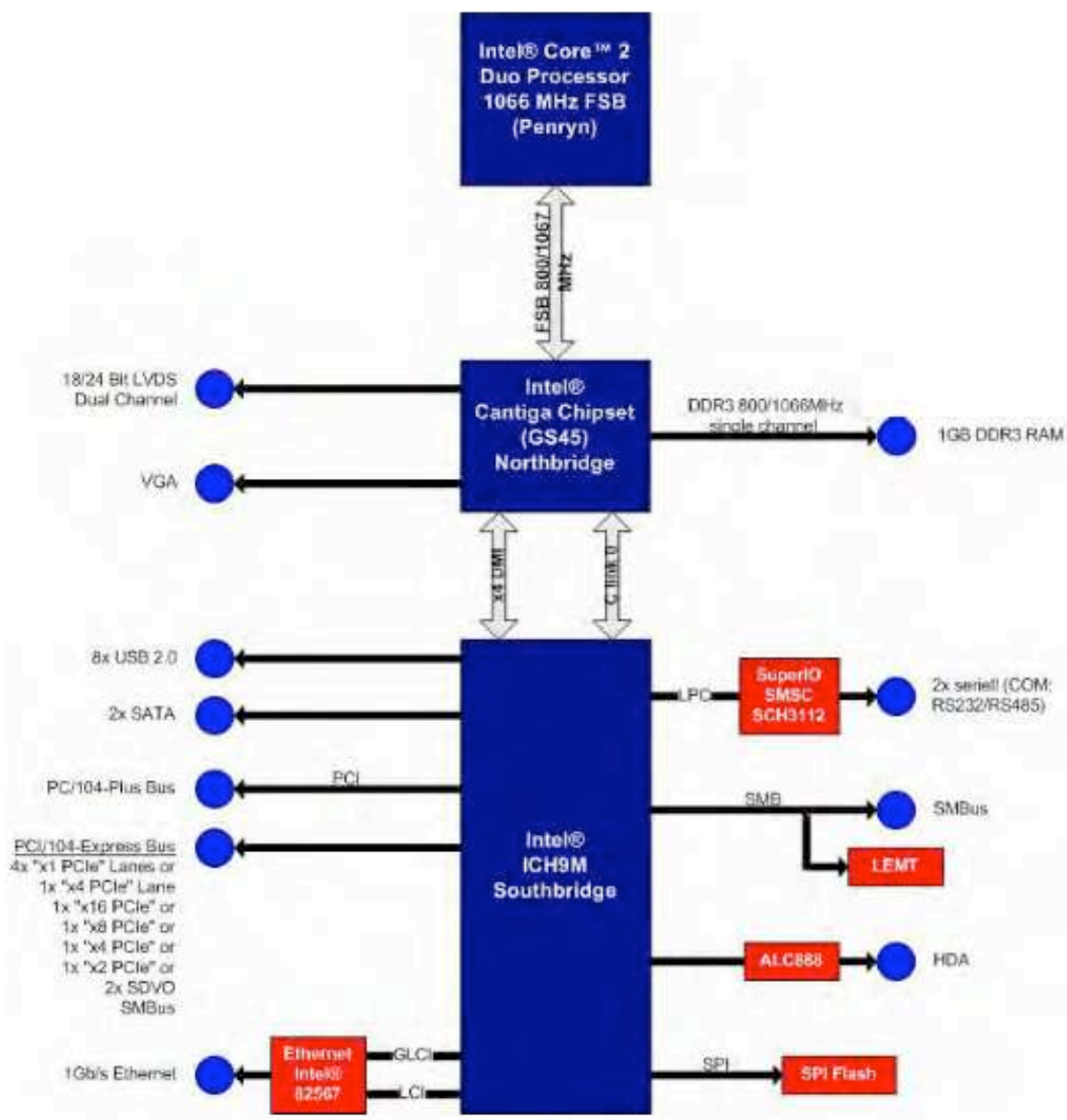


Figure 12: Lippert GS-45 Computer Block Diagram

the heat dissipated by the computer system away from the PC/104 Express stack, reducing demands on the cooling system. With the drive mounted outside of the stack, it would also be easier to remove the disk drive from the payload and recover data if the computer were to become damaged. Thus, the Lippert GS-45 board with external SATA ports will be chosen for this design.

Interfacing the Lippert GS-45 computer with the MOSES instrument could be accomplished in at least two ways. MOSES I used an I/O board produced by RPA Electronic Solutions, Inc. called the “PC/104 FIO” board. On the board, a user-programmable Altera FPGA interfaced 104 GPIO lines with the PCI bus in a PC/104+ stack. The PCI/104 Express standard is backwards compatible with the PC/104+ bus, so this board is still usable. However, a user-programmable FPGA is not strictly necessary, and the usage of such increases the project’s engineering overhead substantially. An externally clockable digital I/O board with 16 TTL inputs could interface with the ROE. The DM9820HR digital interface board from RTD Embedded Technologies has 48 GPIO lines and can be clocked externally up to 25 MHz. This is well above the 2 MHz clock rate of the MOSES I ROE interface. Additionally, the board has two independent DMA channels and two 4MB FIFOs, which should reduce the real-time demands on the CPU. With a 2M word buffer, the CPU can wait up to one second before reading data from the ROE without losing any data. The board can also be used to interface with the 30 GPIO lines used to control and monitor the power system, temperature control system, and other systems on the payload. The DM9820HR I/O board looks to be superior to the RPA FIO board for this application.

The next interface to be considered is the crux of the project: the new cameras. The Intevac Microvista cameras use a CameraLink Base interface, and being as there are six of them, a board with multiple CameraLink Base inputs is desirable. The PHOENIX-D48CL-104PE1 from Active Silicon is a PCI/104 Express dual CameraLink Base frame grabber card with a maximum pixel clock of 66 MHz, which fully supports the Microvista's 44 MHz CameraLink Base interface. It interfaces with the computer using a 1x PCIe slot. One important detail is that the guide scope will have to share a frame-grabber board with one of the spectroscopic imager cameras. It has been verified by the manufacturer that a stack of three Phoenix boards supports a configuration with 5 synchronized cameras and one camera operating independently. Also, the software API is thread safe, meaning that multiple threads can operate the same board. This will afford the software team flexibility to design the software as they see fit.

Completing the PCI/104 Express stack will be the COMMTECH SuperFastCom RS422 synchronous serial board, used to stream housekeeping and image data from the guide scope to the WFF93 PCM encoder that drives the rocket's telemetry module. To maximize the resolution and frame rate of the guide scope video feed, it is desired to use the 10 Mbps of throughput available from the telemetry section as efficiently and completely as possible. The SuperFastcom RS422 board can support data rates up to 50 Mbps, so it should not limit the bandwidth of the guide scope video stream.

Finally, the last component of the design is the data storage. Due to the vacuum and vibration environment that the system will be exposed to, a solid state drive (SSD) is required. Fortunately, SSD's have become very popular since the launch of MOSES I and there are a wide variety of consumer devices available that could be modified for this application. Furthermore, the industry is currently advancing at a very rapid pace- the maximum write speed of commercially available SSD's has doubled between 2010 and 2011. Disk drives are standardized, so there are only three choices to make regarding them: form factor, capacity, and speed. If a custom enclosure is used for the disk drive, the form factor is not a driving factor in the design, but smaller and lighter form factors are preferred. Disk drive speed is to be maximized, as this is inversely proportional to the amount of time between exposures. The required disk drive capacity can be estimated by multiplying the expected average data rate of the instruments by the amount of observation time. In this case, recording 10.4 MB/s for 300 seconds will produce 3.1 GB of data. The flight software and operating system in the original MOSES system used 250 MB of disk drive space. Thus, 4 GB of space should be plenty for the data and the operating system. However, the only downside to using a larger drive is an increase in the cost. The CSSD-F120GB2-BRKT solid state drive from Corsair is advertised as having a maximum write speed of 275 MB/s and a capacity of 120 GB. Another issue to consider is that while the disk drive is fast, if both instruments attempt to write data to it at the same time, one may need to wait and data could be lost if it is not buffered in RAM. Multi-order imaging spectrographs must image all of their detectors at the same time, so for this analysis the size of each exposure in bytes is the sum of the size of each of the constituent images produced by the three CCD's. For MOSES I, an image is 12.6 MB,

and an ESIS image is 8.2 MB. At 275 MB/s, it takes 46 ms to write a MOSES I image to disk, and 30 ms to write an ESIS image. MOSES I was not capable of exposing an image and writing data to disk simultaneously because the camera interface and the disk drive shared the PCI bus and the processor was limited to executing one thread at a time.

However, the proposed centralized design uses separate PCIe links and has a multicore processor, so it should be capable of exposing images and writing images to disk simultaneously. With this being the case, the frame rate is limited by the speed that images can be written to disk.

Table 13 shows a proposed PCI/104 Express stackup for the centralized computer design. Although the system uses a vertical stacking form factor, the end result is a star topology. The CPU is the central star, and the interface cards connect via separate PCIe links. With the exception of the RS-422 card, all the interface cards use FPGAs to bridge between the PCIe link and the interface that the card supports. A possible further expansion on this design concept could be to use a reconfigurable computing module instead of a dedicated interface card, supporting multiple interfaces with one piece of standardized hardware.

Table 13: Centralized Design Proposed PCI/104 Express Stackup

Board	Manufacturer	Model	Internal Interfaces	External Interfaces	Mass (g)	Power (W)
RS422 Board	Commtech, Inc.	SuperFSCC-104	PCI	Two RS422 Ports	93	1.5
Dual CameraLink Interface	Active Silicon	PHOENIX-D48CL-104PE1	PCIe x1	Two CameraLink Base ports	92	4.23 ²
Dual CameraLink Interface	Active Silicon	PHOENIX-D48CL-104PE1	PCIe x1	Two CameraLink Base ports	92	4.23 ²
Dual CameraLink Interface	Active Silicon	PHOENIX-D48CL-104PE1	PCIe x1	Two CameraLink Base ports	92	4.23 ²
GPIO Interface	RTD Embedded Technologies, Inc.	DM9820HR	PCIe x1	48 GPIO Lines	100	1.5
CPU	Lippert Embedded Computers	GS-45	PCI Four x1 PCIe lanes	Two SATA 2.0 ports, Gigabit Ethernet, Eight USB Ports, Two RS232/RS485 Ports	110	32.5
Disk Drive¹	Corsair	CSSD-F120GB2-BRKT		SATA 2.0	80	2

¹: The disk drive will not be mounted in the PCI/104 Express stack. It will be mounted in an external bracket.

²: The Phoenix D48CL dissipates 4.23 W when power over CameraLink (PoCL) is not being used.

Distributed Computing Platform

For the distributed computing platform, the design concept is to build a set of computer modules that each perform one part of the total payload operation with the minimum possible power and mass. Each component will be as simple as possible, but many of them will have to be built to perform all of the requisite functions. There are three proposed instruments for the second generation MOSES payload (Moses I spectroscopic imager, ESIS spectroscopic imager, guide scope), and so three different computer systems must be designed, one for each specific application.

The first computer design will be the one that operates the original MOSES instrument. The existing MOSES C&DH system already operates this instrument in an acceptable manner, so it is useful to examine its design to see what can be improved. Table 14 shows the configuration of the MOSES C&DH system during its February 2006 flight. Three boards were used- the Hercules EBX single board computer, the RPA FIO GPIO interface, and an RS422 board which drove the baseband input for a transmitter used to downlink science data. Table 15 shows the mass and power consumption of the MOSES I flight computer. The flight software runs continuously at 100% CPU usage, so it is not a bad approximation to assume that the computer runs at maximum power all the time. One possibly erroneous assumption made is that the FPGA board uses 10 W, the average that was quoted in its user's manual. The FPGA power consumption is heavily dependent on its configuration, and can be as high as 15 W. The payload draws approximately 26.3 W when powered up in the configuration it was in during its 2006 flight with the flight

software executing, and with all modules except the flight computer powered down. Approximately 2 watts of the power consumption can be attributed to the power supplies' quiescent power consumption, and the supplies are quoted to be 90% efficient by the manufacturer. Thus, it is estimated that 21.7 watts of power is dissipated in the flight computer stack. This is very close to the 22 watts that was estimated in table 15 using component data sheets, which supports the estimate of 10 watts for the FPGA board. The design goals for a revised MOSES instrument computer are to minimize the time between exposures and the mass of the system while dissipating less than the 22 watts used by the original system. The system must also support the interfaces listed in table 16.

Table 14: MOSES I Computer Configuration

Board	Manufacturer	Model	Internal Interfaces	External Interfaces
RS422 Board	Commtech, Inc.	2-104-ET	PCI	Two RS422 Ports
Camera Interface	RPA Electronic Solutions, Inc.	PC104 FIO	PCI	104 GPIO Lines
CPU	Diamond Systems Corporation	Hercules EBX	PCI ISA	ATA33 IDE Port ATA100 IDE Port 4 USB Ports 2 RS232 Ports 2 RS232/RS485 Ports 40 GPIO Lines 100Mbps Ethernet
Disk Drive	BitMicro Networks, Inc.	E- Disk 2A33		ATA33

Table 15: MOSES I Computer Mass and Power Consumption

Board	Manufacturer	Model	Mass	Power Consumption
RS422 Board	Commtech, Inc.	ESCC-2-104-ET	93 g	1.5 W
GPIO Interface	RPA Electronic Solutions, Inc.	PC104 FIO	100 g	10 W ¹
CPU	Diamond Systems Corporation	Hercules EBX	285 g	10 W (Max)
Disk Drive	BitMicro Networks, Inc.	E- Disk 2A33	100 g	0.51 W (Max) 0.25 W (Idle)
Totals:			578 g	22 W

¹: Based on an estimate. The power consumption of the FIO board is not measurable while it is in the PC/104+ stack, and it also depends on the configuration of the FPGA. The manual quotes 10 W for an average design.

Table 16: MOSES I Instrument Computer Interfaces

Interface	Connects from	Data Rate
MOSES I Instrument	Read out electronics	32 Mb/s
RS 232/422 Command Uplink	WFF 93 PCM deck	1200 b/s
RS 232/422 Command Downlink	WFF 93 PCM deck	9600 b/s
Instrument GPIO lines	30 GPIO lines on various payload subsystems	N/A

Several single-board computers were considered for this design. Vendors offered boards designed around the AMD Geode LX800 processor, the Intel Pentium M processor, the Atom series of processors, and several others. The boards using the LX800 processor had the lowest power consumption- typically around 5 W. Power consumption minimization is paramount, as the distributed design requires five computers. At the same time, substantial performance increases are possible using the Intel Atom processor and the additional power consumption is possibly not prohibitive. Boards that use the Atom

processor typically dissipate around 12-15 watts, and support interfaces such as SATA and PCI express which can speed up the system's performance substantially. Three computers that were considered are shown in table 17. The Advantech PCM4153 board was considered initially, but with its slow ATA33 disk drive interface, it was dropped from consideration. The Lippert Cool SpaceRunner-LX800 has the lowest power consumption of the boards that were considered, but it also has the lowest amount of RAM, a slightly slower onboard solid state disk drive (SSD), and it lacks onboard RS422 ports. RTD's low power offering has the optimal amount of RAM for this application, an optional 8 GB onboard solid state drive that is twice as fast as the one used on the original MOSES system, and two onboard RS422 ports.

The last board considered was the Lippert Cool RoadRunner-945GSE, an Atom based board. It supports SATA, so disk drives that are 20 times faster than the one used on the original MOSES instrument can be used. Using Amdahl's law, this would reduce the exposure cycle for the original MOSES instrument from 9.18 to 8.33 seconds. Using the Atom-based computer and a SATA disk drive would dissipate 9.75 W more than using the Lippert LX800 based machine, which would require 247 more grams of batteries and the addition of 1.33 kg of aluminum heatsink material. This would reduce the observation time by 1 second. During the flight of the original MOSES C&DH system, the minimum guaranteed observation time was 283 seconds and the system completed a three second exposure in 9.18 seconds (It took six seconds to store the data), so the system could take 30 exposures. With all other hardware staying the same, the Atom-based system could complete thirty-four 8.33 second exposure cycles in the same amount of time.

Table 18 shows three possible configurations for a computer to run the MOSES instrument. The Lippert Cool SpaceRunner and the RTD CME137686LX500HR-512 are very similar machines and have similar performance. The RTD computer does include onboard RS422, however, and saves some power and mass by not needing an extra RS422 card. The last machine, the Lippert Cool RoadRunner, weighs twice as much and has a disk drive that is 20 times faster than the other two machines. The exposure cycle is limited mostly by the optics and the readout electronics however, and thus it cannot make up enough time to justify its bulk. Between the two remaining machines, the RTD computer is both lighter and faster, so it is the clear choice.

Table 17: Low Power Single Board Computers for the MOSES I Instrument

Manufacturer	Model	Processor	Ram	Onboard SSD	Serial Ports	Disk Drive Interface	Power Consumption¹	MTBF
Lippert Embedded	Cool SpaceRunner-LX800 PC/104 +	AMD Geode LX800, 500MHz	256 MB, DDR400	2 GB, 20 MB/s Write 30 MB/s Read	2x RS232/RS485	ATA100	4.75 W (Max) 3 W (Idle)	294,173 Hours @ 25 °C
RTD	CME137686 LX500HR-512 PC/104 +	AMD Geode LX800, 500MHz	512 MB, DDR333	2,4, or 8 GB 30 MB/s Write 40 MB/s Read	2x RS232/RS422/RS485	ATA100	5.7 W (Typical)	115,000 Hours @ 23 °C
Lippert Embedded	Cool RoadRunner-945GSE PC/104 +	Intel Atom N270 1.6 GHz	1 GB DDR2 533MHz	2 GB, 20 MB/s Write 30 MB/s Read	2x RS232/RS485	2x SATA 300 MB/s	12.5 W (Max) 9.5 W (Idle)	159,899 Hours @ 25 °C

¹: The exact circumstances during which these numbers were measured are not listed in the product manuals. They are reproduced here as they were listed by the manufacturer.

Table 18: Three Possible MOSES Instrument C&DH Stacks

Computer	Serial Interface	MOSES Instrument Interface	Disk Drive	Total Power Consumption	Required Heatsink Mass	Required Battery Pack Mass	Incremental decrease in Observation Time	Predicted Exposure Cycle Length
Lippert Cool SpaceRunner-LX800 100 g, 4.75 W	CommTech Super Fastcom 93 g, 1.5W	DM7820HR 100 g, 1.5 W	Onboard SSD	7.75 W	1.30 kg	196.2 g	1.112 s	8.91 s
RTD CME137686L X500HR-512 130 g, 5.7 W	Onboard	DM7820HR 100 g, 1.5 W	Onboard SSD	7.2 W	1.16kg	182.3 g	0.979 s	8.7 s
Lippert Cool RoadRunner-945GSE 115 g, 12.5 W	CommTech Super Fastcom 93 g, 1.5W	DM7820HR 100 g, 1.5 W	Corsair CSSD-F120GB2-BRKT 80 g, 2 W	17.5 W	2.42 kg	392.4 g	1.944 s	8.326 s

The distributed design calls for five computer stacks to be built for the operation of ESIS. Each one will interface with one of the detectors through an Arvio Orlando CL PC/104 + CameraLink board. This CameraLink interface can be externally triggered using a GPIO line, so all of ESIS's five CCDs can be triggered simultaneously. Debugging and housekeeping telemetry could be output from each machine via either serial or Ethernet. The computers listed in table 17 were again considered for this application. In this application the computers are not multitasking, and buffering image data in RAM is less of a concern. Each 1 s exposure produces only 1.6 MB of data, so the amount of memory needed will be driven primarily by the operating system. All the systems being considered have ample memory for a small Linux distribution, so RAM will not be a large factor in the design. For a 300 second flight, approximately 500 MB of disk drive space would be necessary to store the data. Along with 250 MB for the operating system and software, 750 MB of space would be needed. All the systems considered have at least 2 GB of space, so this parameter is also not expected to drive the design.

The write speed of the disk drives is an important factor though, as the disk drive must be capable of writing images to disk as fast as they are captured. The disk drive limits the maximum frame rate that can be achieved. With a 1.6 MB image, the Lippert Cool SpaceRunner- LX800 would take 80 ms to store an image. The RTD CME137686LX500HR-512 would require 53 ms, and the Lippert Cool RoadRunner- 945GSE with an external SATA SSD would require just 6 ms. It takes 33 ms to readout an exposure. The LX800 based machines use a PCI-based IDE controller, which means that the computer cannot simultaneously read data from the frame grabber board and

write to the disk drive, since the bus is shared. The Cool RoadRunner-945GSE uses a dedicated I/O controller (The Intel ICH7M), and the disk drive interface doesn't share a bus with the CameraLink board. It can thus write images to disk and readout new images in parallel. The frame rate for that machine is limited by the frame grabber, since it is slower than the disk drive. Table 19 compares the delay between exposures for each configuration and the incremental decrease in observation time for each computer. This is defined as the amount of observation time that would be lost if the 1046 lb version of the payload was flown, with the original MOSES flight computer removed and the test computer installed. The batteries and heat sinks would be resized for the new configuration, but all other hardware would remain the same.

Table 19: Three Possible ESIS Computer Configurations

Computer	Cameralink Interface	Delay Between Exposures	Number of 1 s Exposures in 283 s	Incremental Decrease in Observation Time Per Unit	Incremental Decrease in Observation Time Per 5 Units
Lippert Cool SpaceRunner-LX800 100 g, 4.75 W	Arvoo Orlando CL, 100 g, 2.5 W	0.113 s	254	0.97 s	4.83 s
RTD CME137686 LX500HR-512 130 g, 5.7 W	Arvoo Orlando CL, 100 g, 2.5 W	0.086 s	260	1.09 s	5.43 s
Lippert Cool RoadRunner-945GSE 115 g, 12.5 W	Arvoo Orlando CL, 100 g, 2.5 W	0.033 s	274	2.10 s	10.48 s

The difference in performance between the three machines is fairly minimal, although the performance of the individual pieces of hardware varies over a large range. Using a 1 s exposure, the slowest computer considered only affects ~10% of the total exposure cycle time. The computers are much faster than the detectors can gather photons.

One factor that does scale directly with computer performance is the incremental decrease in observation time. In particular, the use of the Cool RoadRunner-945GSE would eliminate 10.48 s of observation time. While this is only 3.3% change in the observation time, it has to be considered that there is other hardware not included in this analysis that will reduce the observation time as well. Because of this, the Cool RoadRunner-945GSE is not a good option for this application. The RTD CME137686LX500HR-512 can capture 95% as many exposures as the Atom-based CPU and has half as much of an effect on the observation time. It also has RS422 ports onboard, a feature lacking in the otherwise comparable Lippert Cool SpaceRunner-LX800. A computer stack consisting of the RTD CPU and an Arvoo Orlando-CL CameraLink interface will be used for this design.

The final computer to be designed is the guide scope computer. The only functional difference between it and one of the ESIS machines is that it must also output image data to the WFF93 stack via synchronous RS422. This can be facilitated by adding a CommTech SuperFASTComm RS422 interface to the PC/104+ stack. The complete distributed system design is shown in table 20.

Table 20: Distributed Computer System Design

Instrument	Number of Units Needed	CPU	Serial Interface	Camera Interface	Disk Drive
MOSES	1	RTD CME137686L X500HR-512 130 g, 5.7 W	Onboard	DM7820HR 100 g, 1.5 W	Onboard SSD
ESIS	5	RTD CME137686L X500HR-512 130 g, 5.7 W	Onboard	Arvoo Orlando CL, 100 g, 2.5 W	Onboard SSD
Guide Scope	1	RTD CME137686L X500HR-512 130 g, 5.7 W	CommTech Super Fastcom 93 g, 1.5W	Arvoo Orlando CL, 100 g, 2.5 W	Onboard SSD

With seven computers using a total of 15 circuit boards, the distributed system would increase the volume of the C&DH system substantially. The densest possible configuration would be to integrate the computers into one stack, using 1.5” spacers between separate computers so that they did not connect to each other. The PC/104+ specification calls for 0.6” spacing between boards within the same stack, so the total length would be 14.4”. Figure 14 shows the end of the payload that contains the flight computer, which is mounted in the large box in the center of the image. There is room for a second computer enclosure of similar dimensions below and to left of the existing computer. MOSES used a Hercules EBX form factor motherboard, which was 8” long, so it should be possible to fit an 8” stack of PC/104+ boards in the enclosure if they were mounted perpendicular to the optical table. With two boxes, there would be enough space

for 16” of stacked computers, which should fit the distributed system. It may be necessary to extend the box a few inches to facilitate cable routing, however.

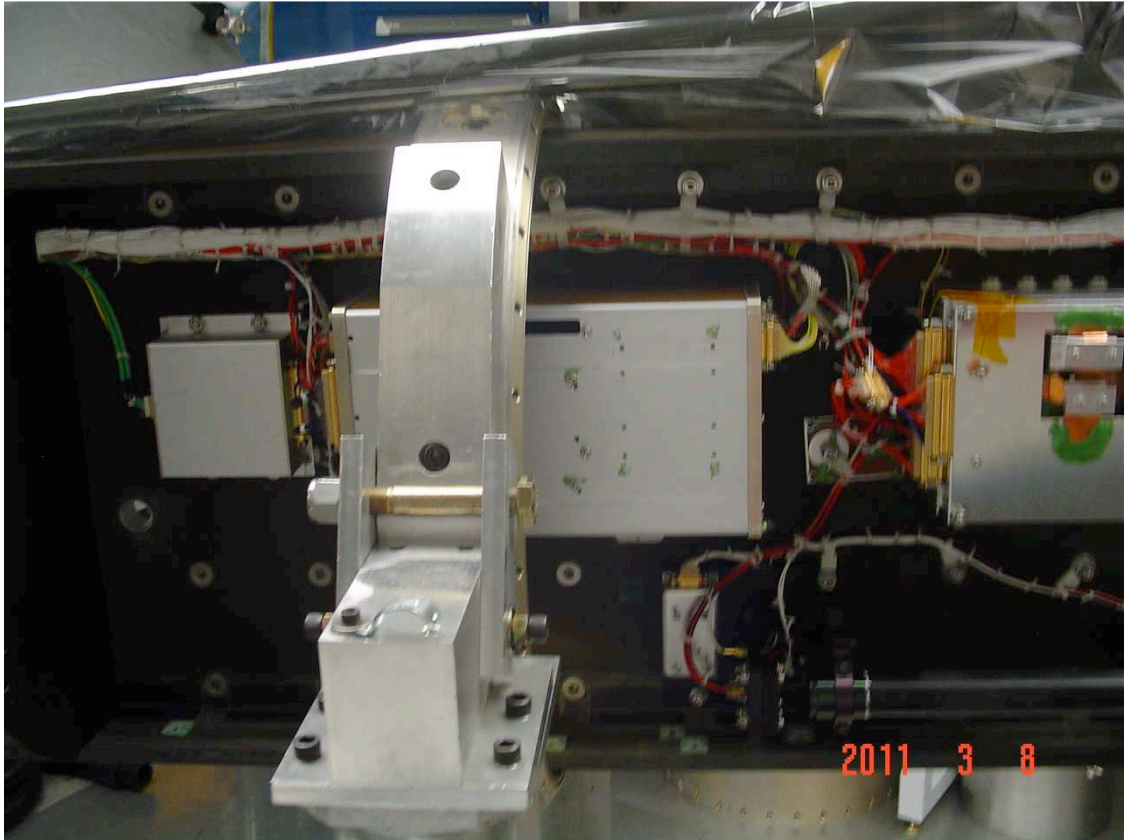


Figure 14: The end of the MOSES payload containing the computer

One final consideration is that all seven of the computers in the distributed system must be controllable from one external computer for debugging purposes. This could be accomplished by routing Ethernet ports from each machine through the payload umbilical and into a network switch located with the rest of the ground support equipment (GSE).

A dedicated router could be used, or a computer in the GSE rack could be setup to route packets on the network.

Conveniently, it was the case that the same CPU was a good fit for all three computer configurations. This was unintentional and not strictly necessary, but this would reduce the amount of effort required from the software engineers substantially. A large amount of the software could be reused for each system, and development costs could be reduced by buying only one software development kit. A substantial savings in both time and money is possible by using a uniform set of hardware.

PERFORMANCE OF THE TWO SYSTEMS

In this chapter, the performance of the two systems will be compared to find out which one better suits the needs of the second-generation MOSES payload. This chapter will begin with a section describing the design metrics being used in detail. Then, comparisons will be drawn and finally the paper will draw to a close with a chapter full of conclusions about the designs.

A sounding rocket can be thought of as a chemically powered electromechanical device that provides observation time above a specific altitude. At the end of the launch there is only data and memories. The quality of a sounding rocket payload system design can thus be thought of as being proportional to the quality and quantity of the data retrieved divided by the amount of effort it took to capture it, which can be measured in both time and money. The optics largely dictate the quality of the data, but the C&DH system can facilitate the addition of more instrumentation and increase the breadth of the information gathered. The instrumentation was chosen at the outset of this study, so the remaining variables are the quantity of data captured and the effort it would take to capture it.

The amount of data captured is a function of the observation time and the speed at which the images are captured. However, it is not within the scope of this study to synthesize entire payload designs. Because of this, the final payload mass and thus the observation time is unknown. However, in the 2006 flight of MOSES, the sounding rocket program listed a minimum observation time of 283 s as part of the minimum success criteria,

guaranteeing at least that much observation time. Assuming that this would be the case for future flights of the MOSES payload, one useful design metric is the number of exposures the payload can complete within 283 seconds.

It is highly likely that the payload will be able to observe for more than 283 seconds, however, and it would be useful to capture the impact of the C&DH system's mass on the "extra" observation time. The derivative of the mass vs. observation relationship found in chapter 1 was determined numerically, and it was found that within a small range around 1046 lbs, the payload loses 0.28 seconds of observation time per pound (or 0.62 seconds per kg) of mass it gains. The total observation time would be necessary to predict the total number of exposures for the flight, but the two pieces of information that are available can be used to choose a flight computer implementation.

A key part of the calculation is the mass of the C&DH system, which is comprised of the mass of the components themselves, the batteries required to power them, and the heat dump required to cool them. The masses of the components were found from their datasheets. An important consideration is that the boards will be modified for flight, which will change their masses. Figure 15 shows a flight modified PCI/104+ board that was used in the early design stages of MOSES I that did not make it to the final flight build. Shown with extra attached cabling, its weight should be representative of what would be expected of a flight board, which will have copper heat sinks, heat pipes, and external cabling installed. The mass is 196 g, approximately double that which was specified for the unmodified PCI/104 Express boards. This extra mass is almost entirely due to the

copper heat blocks that were installed to thermally connect heat pipes from the electronics to aluminum heat dumps. There was no exact procedure regarding the design of these blocks, so this study will assume that there is 100 grams of copper added to each board.



Figure 15: Flight Modified PC/104+ Board

Table 21 shows the mass and power consumption of each of the components used in the centralized design. Summing the mass of each of the components yields a total mass of 659 g. The average power consumption will be 26.2 W, and the maximum power consumption will be 50.2 W. However, this only includes the PCI/104 Express stack and the disk drive- the cameras will consume power, and there are additional support

electronics (temperature gauges, current sensors, voltage sensors, etc.) that will consume power, but these are not designed yet and are thus not included in this study. Table 22 shows the same information for the distributed computer.

Table 21: Centralized Computer Mass and Power Consumption

Board	Manufacturer	Model	Mass	Power Consumption
RS422 Board	Commtech, Inc.	SuperFSCC-104	93 g	1.5 W
Dual CameraLink Interface	Active Silicon	PHOENIX-D48CL-104PE1	92 g	4.23 W (Not using power-over-CameraLink)
GPIO Interface	RTD Embedded Technologies, Inc.	DM9820HR	100 g	1.5 W
CPU	Lippert Embedded Computers	GS-45	110 g	32.5 W
Disk Drive	Corsair	CSSD-F120GB2-BRKT	80 g	2 W
Totals:			659 g	50.19 W

Table 22: Distributed Computer Mass and Power Consumption

Computer	Board	Manufacturer	Model	Mass	Power Consumption
MOSES	CPU	RTD Embedded Technologies, Inc.	CME137686LX500HR-512	130 g	5.7 W
	GPIO Interface	RTD Embedded Technologies, Inc.	DM7820HR	100 g	1.5 W
Totals:				230 g	7.2 W
ESIS	CPU	RTD Embedded Technologies, Inc.	CME137686LX500HR-512	130 g	5.7 W
	CameraLink Interface	Arvoo	Orlando CL	100 g	2.5 W
Totals:				230 g	8.2 W
Guide Scope		RTD Embedded Technologies, Inc.	CME137686LX500HR-512	130 g	5.7 W
	GPIO Interface	RTD Embedded Technologies, Inc.	DM7820HR	100 g	1.5 W
	High Speed Serial Interface	CommTech	FastComm	93 g	1.5 W
	CameraLink Interface	Arvoo	Orlando CL	100 g	2.5 W
Totals:				423 g	11.2 W
System Total:			All seven computers:	1,803 g	59.4 W

The mass of the distributed system is approximately three times more than the centralized system, because there are three times as many circuit boards. The power consumption is comparable, with the distributed system using 18% more power than the centralized system.

The next component of the mass that will be considered is the heat dumps. The required mass of aluminum necessary to cool the electronics during the flight can be calculated using equation 4:

$$(C_d * M_d + C_p * M_p + C_b * M_b) \frac{T_r}{\tau} = P \quad \text{Eq. 4}$$

Where:

C_d is the specific heat of the aluminum heat dump in $\text{J g}^{-1} \text{K}^{-1}$.

M_d is the mass of the aluminum heat dump in g.

C_b is the specific heat of the aluminum box housing the computer in $\text{J g}^{-1} \text{K}^{-1}$.

M_b is the mass of the aluminum box housing the computer in g.

C_p is the specific heat of the copper heat pipes in $\text{J g}^{-1} \text{K}^{-1}$.

M_p is the mass of the copper heat pipes in g.

P is the maximum power dissipation in watts.

T_r is the allowable temperature rise in Kelvins.

τ is the time from when the rocket is disconnected from launch pad cool systems to when it is powered down in seconds.

The specific heat of aluminum is $0.897 \text{ J g}^{-1} \text{K}^{-1}$, and for copper it is $0.385 \text{ J g}^{-1} \text{K}^{-1}$. In chapter 3, figure 11 shows the first MOSES flight computer, with an aluminum manifold for mounting heat pipes on the right side. An aluminum plate below the electronics box was used as a heat dump, in addition to a cold finger protruding from the opposite side of the optical table. However, its mass wasn't documented. Figure 16 (reproduced from an internal group report) shows data from a thermal test that was run in 2005 with the MOSES flight computer. It was powered up and the temperature was measured as it was

operated in vacuum for 20 minutes. During the last 5 minutes of the test, the temperatures of the components tracked that of the aluminum heat dump, which rose at a rate of one degree every five minutes. Equation 4 was used to determine that approximately 3 kg of aluminum was conductively coupled to the flight computer, under the assumption that 400 g of copper was used to interface the electronics with the heat dump. Measurements taken of the flight computer enclosure on show that the volume of aluminum used in its structure is approximately 1,159 cm³. The density of Al is 2.7 g / cm³, so using this method the mass is 3,130 g. The difference between the number calculated from the thermal test and the one calculated using the volume is within the expected error, given that the volume measurements were done with a tape measure and the enclosure was sealed, barring the measurement of some features. The close agreement of the two methods (<5% difference) indicates that equation 4 is accurate enough for this application despite being a simplified thermal model. Heat dumps for the second generation MOSES payload will be sized to maintain the system's current rate of temperature change, 0.0033 kelvin per second.

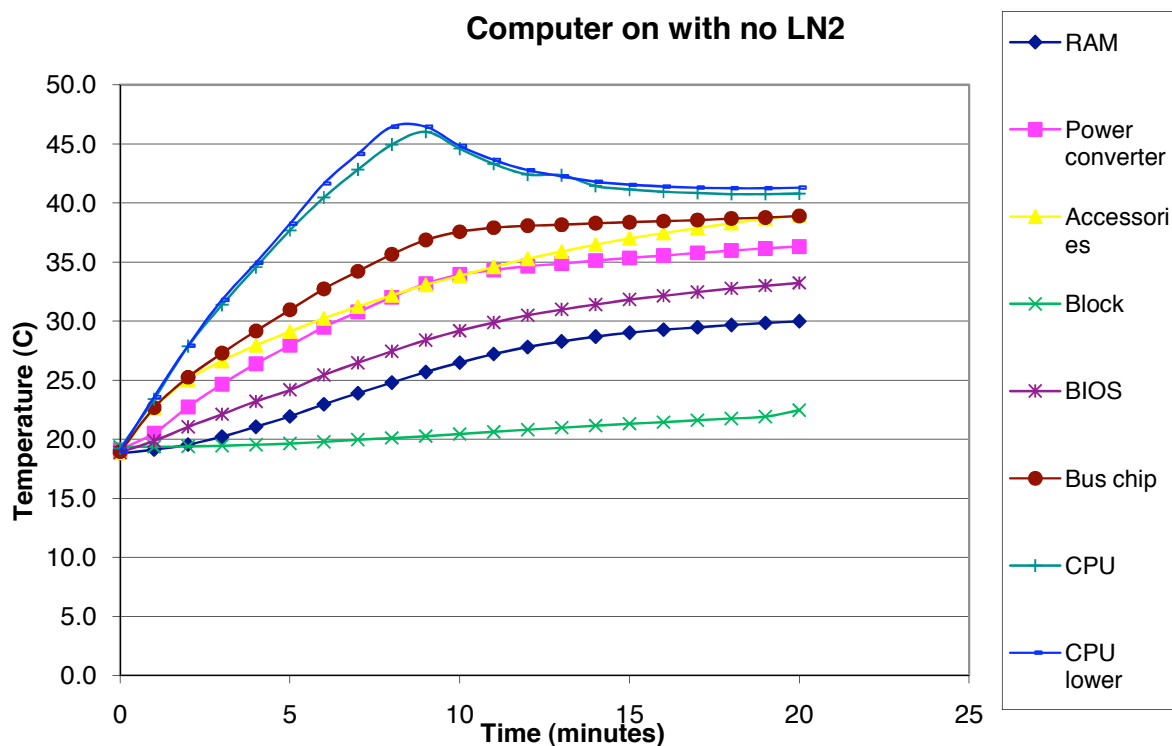


Figure 16: 2005 Moses Flight Computer Thermal Test Data

One last consideration is the size of the batteries necessary to run the payload. The sounding rocket program handbook lists several configurations of batteries, their capacities, and their masses. On average, the packs provide 11.44 watt-hours of electricity at 28 V per pound of battery pack mass. With the application of some algebra, it can be found that this is equivalent to 0.025 watt – hours per gram. This is an abstraction, as batteries are only available in discrete sizes, but it can be used to compare two systems. This approximation is necessary, because the total power consumption for all the electronics can't be determined until the entire payload is designed. The MRR from the first flight of MOSES (Payne, 2006) included a power budget which was based on 1,140 seconds of payload operation and power margin of 2 (They flew at least twice

as many batteries as they needed). Thus, for MOSES I it would have been necessary to fly 557 grams of batteries to power the PC/104+ stack. For the centralized design that is proposed, 1.3 kg of batteries would be required to power the PCI/104 Express stack. The distributed system would require 1.5 kg of batteries. The complete masses of both test systems and the original MOSES flight computer are shown below along with their effect on the observation time.

Table 23: Computer System Mass Comparison

System	C&DH stack mass	C&DH stack required heat dump mass ¹	C&DH stack required battery mass	Total mass	Mass per Camera ²	Predicted change in observation time ³	Volume
MOSES I	568 g	3,400 g	557 g	4,550 g	1,517 g	-2.833 s	4.19 L ⁴
Centralized Design	659 g	7,404 g	1,270 g	9,333 g	1,037 g	-5.811 s	3.71 L ⁵
Distributed Design	1803 g	9,483 g	1,504 g	12,790 g	1,421 g	-7.963 s	8.61 L ⁶

¹: Includes the electronics enclosure and the copper heat pipes. This includes 100 g of copper for each board in the system, except for the MOSES I CPU which was a bigger form factor and would need 200 g of copper.

²: For MOSES I, three cameras were controlled by the C&DH system. For MOSES II, 7 cameras are controlled by the C&DH system.

³: The amount of observation time that would be lost compared to flying the 1046 lb version of the payload with no flight computer.

⁴: Calculated using the dimensions of its enclosure.

⁵: Calculated using the volume of the PCB stack plus an inch on all sides for cable routing. An extra inch of space at the top of the PC/104 Express stack was allotted for the disk drive.

⁶: Calculated using the volume of the PCB stack plus an inch on all sides for cable routing.

The performance of the two test computer systems and the original MOSES flight computer is summarized in table 24. Both computers can take images significantly faster

than ESIS's nominal rate of 1 frame per second, and the difference in their performance with the MOSES instrument is negligible. The distributed system is clearly more massive than the centralized system and costs the payload an extra 2.19 seconds of exposure time. However, the standard deviation in the observation time for this payload configuration is 9 s (Sounding Rocket Program Office, 2001), and thus it has to be asked whether a difference of 2.19 s is significant. This is especially true given that extra, unaccounted for mass on the order of 50 lbs was added to the payload during its first flight for reentry stability. One important thing to note is that the payload mass and the observation time lost because of it is not a random variable. Although the effect due to the C&DH system is much smaller than the error and the uncertainty in the flight time, its effect would still be there regardless of external factors, unless the minimum expected observation time were to fall below 283 s. In that case, the configuration of the rocket would be altered to guarantee the minimum observation time.

Table 24: Centralized Vs. Distributed System Performance

System	Delay Between MOSES Exposures	Number of 3 s MOSES Exposures in 283 s	Maximum ESIS Frame rate	Number of ESIS Exposures in 283 s	Predicted change in observation time³
MOSES I	6.18 s	30.83	-	-	-2.787 s
Centralized Design	4.75 s	36.52	33.34 fps	9,435	-5.811 s
Distributed Design	5.12 s	34.85	18.31 fps	5,182	-8.000 s

In both designs, the limiting factor in the frame rate was the write speed of the hard drive. Neither design came close to saturating the expansion port busses (PCI and PCI Express),

or the CPU's front side bus. In the "Distributed Computer" section on page 72, it was found that upgrading to a computer with a fast SATA disk interface could increase the frame rate, at a cost of increasing the power consumption and thus losing some observation time.

Earlier in this section it was stated that the quality of the system is a function of the quality and quantity of the data it produced and the effort it would take to build the system, but not much has been said about the latter. Once the computer hardware arrives in the lab, the remaining tasks are to write software, design and build the enclosure(s), and integrate the system. The two systems pose unique challenges in each of these categories.

The centralized system requires multitasking software with soft real-time capabilities, whereas the distributed system uses three different applications which still must implement a soft real-time system, but are not multitasking, with the exception of the MOSES instrument computer which performs housekeeping functions. Thus it is expected that the software for the centralized system will be more difficult to implement, but the distributed system would require more of it. It will be desirable to match the hardware design with the skill level and number of programmers available to work on the project to hasten software development.

For the mechanical engineers, the distributed system will likely be the more difficult of the two systems to work with. Using two enclosures as proposed earlier in this chapter, it will double their workload in both the design and fabrication stages unless a design can be found that accommodates both computer stacks, which will be configured differently. Machine shop time can also be very expensive – the enclosures will almost certainly cost more to produce than their contents. The distributed design also occupies a larger volume, reducing the free space that is available for other systems and possibly further complicating any new systems added to the payload.

After the software and enclosure have been built, the system must be integrated into the payload. This task scales with the number of boards in the system, as copper heat sinks and heat pipes must be fabricated to interface the system to its heat dumps. Each board must also be modified for flight, a process which includes replacing parts that won't survive vacuum and installing thermistors. Larger components on each board are also staked down with epoxy. Most likely, the biggest task will be building and installing the wire harnesses that connect the system together. Vacuum compatible cabling is difficult to obtain, thus all cables must be built in-house, by hand. This is another category in which the centralized computer is superior to the distributed one.



SUMMARY, CONCLUSIONS, AND FUTURE WORK

Space-borne spectroscopic imagers can provide an insight into solar activity that is not available to terrestrial observers. The atmosphere is opaque at EUV wavelengths, which makes observation of the sun's higher energy features impossible from the surface of the Earth. Sounding rockets provide a platform upon which an instrument can be launched above the atmosphere, and the MOSES group has chosen a EUV spectroscopic imager as the instrument for this project. This instrument simultaneously captures images, spectral line profiles and velocity maps of the transition region of the sun unambiguously, providing a wealth of scientific information.

The current MOSES and the proposed ESIS instruments use a synchronized array of detectors together with a multi-layer coated concave diffraction grating to perform spectroscopic imaging. A narrow range of optical wavelengths is passed by the multi-layer coatings, which limits the ability of the instrument to observe multiple spectral lines, but prevents the ambiguity of the produced image. To simultaneously observe multiple spectra lines it is necessary to use multiple instruments.

However, the current MOSES C&DH system cannot support multiple instruments without significant reduction in its frame rate. A new C&DH system must be built to support the additional detectors needed for a multi-instrument system. A centralized and a distributed computer system have been designed and compared to see if either provides significant advantages over the other.

To aid in the redesign, guidelines were extracted from publications on the experience of the launches of MSSTA and MOSES. The MSSTA team used the same camera for all of their instruments, a move that saved them time getting their telescope array to the launch pad. Also, since film was used as the sensing media, there was no need to handle data on board the sounding rocket. CCDs have superior performance, however, and were used in the MOSES instrument. The CCDs used a nonstandard interface and extra circuitry in the form of a deserializer and an FPGA were necessary to input the data to the flight computer, which increased the mass and power consumption of the payload. It was found that the time to launch and the amount of hardware in the payload could be reduced by using a homogenous array of cameras with standard interfaces.

A suite of cameras using CMOS detectors was chosen for the ESIS instrument. Although they have less dynamic range than CCDs, they offer faster frame rates and the ability to be read out at multiple resolutions. CMOS detectors can be read out, flushed, and exposed line-by-line, which eliminates the need for a mechanical shutter as well. CMOS detectors offer more flexibility than CCDs, which is an important factor considering that the camera must be capable of functioning in multiple instruments.



Two computer designs were synthesized and analyzed. The first one was based on a centralized computer, using a star network. Cameras connected to the computer using CameraLink interface cards which were installed in the computer's PCI Express ports. PCI Express was chosen for an expansion port bus because it is a point-to-point serial

connection, so the CPU can control multiple PCIe devices simultaneously. This is necessary so that instruments don't waste observation time during flight waiting for access to a PCI bus. The most important consideration for the centralized computer system is the number of expansion ports, their bandwidth, and how data flows through the system.

The software is expected to not be very CPU intensive, but there are multiple threads that need to operate in near real-time. This drove the decision to use a multi-core processor with a low clock speed. However, this did mean that the system was forced to use more RAM than was absolutely necessary since boards with multi-core processors and 512 MB of RAM didn't exist on the market.

Next, a distributed system was considered that avoided multitasking by pairing each detector up with a dedicated computer. Emphasis was placed on reducing power consumption, as the mass increase due to upgrading any part of the computer system is multiplied by the number of computers used. Since the computer did not need to control multiple peripherals simultaneously, the PCI bus could be used for this design. This allowed the design to use the PC/104+ form factor, which vastly reduced the power consumption per computer when compared with the centralized system.



However, it was found overall that the centralized system is both faster and lighter than the distributed system. The distributed system is more massive because hardware is redundantly copied on each computer. Where there only needs to be one voltage



regulator, there is seven, etc. The centralized system uses 1 GB of RAM, whereas the distributed system contains 3.5 GB altogether. This extra hardware increases the power consumption and the required heat dump mass as well.

The performance of the two computer systems was found to be limited by the disk drive write speed, as the expansion port busses used are much faster than the instrument data rates. This allowed the centralized system to outperform the distributed system by using a SATA hard drive that was 10 times faster than the PATA disks used in the distributed system. The mass required to upgrade the distributed system to SATA hard drives was found to be substantial. However, the performance increase would be prodigious.



The upgrade is not warranted, given that the overall system performance is limited by the time necessary to acquire an exposure. Both systems considered can acquire ESIS images at a rate faster than 10 fps, but it is expected that it will take at least 1 s to acquire an



acceptable exposure. Also, their performance with the MOSES instrument is very similar. Thus, the main factors driving the decision between the two machines are their affect on the observation time and the difficulty with which they can be built. It was established earlier that the distributed system has a larger effect on the observation time, so the remaining consideration is the amount of engineering effort required to build the system.

Performing more tasks than the distributed system with less hardware, the centralized system is more complex. It will require more skillful programming. However, the



distributed system will require a larger amount of software and also more mechanical

hardware and support electronics will be required. The size and skillset of the engineering teams implementing the system would have to be considered to determine which design is better from a manufacturability standpoint. Given the MOSES group's previous success with the current system (which is most similar to the centralized computer), the logical choice would be to build a centralized system. This system is the faster of the two considered, the lightest, and its design builds upon the group's previous work.

FUTURE WORK

To move forward from this study, a first step might be to build and verify the performance of the two systems proposed herein. Particularly, it would be prudent to establish that there are no unknown incompatibilities between the pieces of hardware used and that the systems operate as described. Also, it could be insightful to design a  third system based on a mixed topology- a distributed array of centralized systems. This could reduce the amount of redundancy in the distributed system and reduce the system's complexity by dividing its functionality among two or more systems. One last area that might be interesting to consider is how the designs scale as the number of ESIS detectors is changed. This would seek to determine how the mass, power consumption, and frame  rate change as ESIS is scaled to 3,5 or 7 detectors.